

Ab initio study of the beryllium isotopes ${}^7\text{Be}$ to ${}^{12}\text{Be}$

Shihang Shen,^{1,2} Serdar Elhatisari,^{3,4,5} Dean Lee,⁶ Ulf-G. Meißner,^{5,2,7,1,*} and Zhengxue Ren²

¹Peng Huanwu Collaborative Center for Research and Education, Beihang University, Beijing 100191, China

²Institute for Advanced Simulation (IAS-4), Forschungszentrum Jülich, D-52425 Jülich, Germany

³Interdisciplinary Research Center for Industrial Nuclear Energy (IRC-INE),

King Fahd University of Petroleum and Minerals (KFUPM), 31261 Dhahran, Saudi Arabia

⁴Faculty of Natural Sciences and Engineering, Gaziantep Islam Science and Technology University, Gaziantep 27010, Turkey

⁵Helmholtz-Institut für Strahlen- und Kernphysik and Bethe Center for Theoretical Physics, Universität Bonn, D-53115 Bonn, Germany

⁶Facility for Rare Isotope Beams and Department of Physics and Astronomy,

Michigan State University, East Lansing, MI 48824, USA

⁷Tbilisi State University, 0186 Tbilisi, Georgia

We present a systematic *ab initio* study of the low-lying states in beryllium isotopes from ${}^7\text{Be}$ to ${}^{12}\text{Be}$ using nuclear lattice effective field theory with the $N^3\text{LO}$ interaction. Our calculations achieve excellent agreement with experimental data for energies, radii, and electromagnetic properties. We introduce a novel, model-independent method to quantify nuclear shapes, uncovering a distinct pattern in the interplay between positive and negative parity states across the isotopic chain. Our geometrical analysis reveals prominent two-center cluster structures, the emergence of one-neutron halo, and complex nuclear molecular dynamics, underscoring the strong clustering features inherent to beryllium isotopes.

INTRODUCTION

Beryllium isotopes are pivotal in nuclear structure studies due to their diverse phenomena, including clustering, halo structures, and the breakdown of conventional shell closures. For instance, ${}^7\text{Be}$ plays a significant role in Big Bang nucleosynthesis and nuclear astrophysics by influencing the primordial abundances of light elements [1, 2]. The unbound ${}^8\text{Be}$, which decays into two alpha particles with a long lifetime, exemplifies nuclear instability and clustering effects. Moving along the isotopic chain, ${}^9\text{Be}$ and ${}^{10}\text{Be}$ are renowned for their pronounced molecular-like structures [3]. The neutron-rich ${}^{11}\text{Be}$ is particularly notable for its ground-state parity inversion and halo structure, challenging traditional shell-model predictions and providing insights into weakly bound systems [4, 5]. Similarly, ${}^{12}\text{Be}$ exhibits the disappearance of the $N = 8$ shell closure, highlighting the role of intruder configurations and shape coexistence [6–9]. The spectra of ${}^{10}\text{Be}$ and ${}^{11}\text{Be}$ have been used early to test the chiral three-nucleon forces (3NFs) in nuclei [10]. These rich and varied phenomena underscore the need for comprehensive theoretical frameworks capable of capturing the complex interplay of clustering, shell evolution, and continuum effects in beryllium isotopes.

A variety of theoretical approaches have been employed to study these isotopes, with significant emphasis on cluster structures, such as Antisymmetrized Molecular Dynamics (AMD) [11–17], Fermionic Molecular Dynamics (FMD) [18], molecular-orbital models [19, 20], the Tohsaki–Horiuchi–Schuck–Röpke (THSR) wave function approach [21–23], and other cluster models [24–35]. These methods have effectively captured cluster structures, molecular configurations, and the influence of valence neutrons in beryllium isotopes. See also the recent reviews [36–39]. In parallel, density functional theory has been employed to predict the formation of alpha clusters bonded by

excess neutrons, highlighting the significant role of clustering in these systems [40–42]. *Ab initio* methods such as the Gamow shell model [43], Green’s function Monte Carlo [44–49], the resonating group method [50], Monte Carlo shell model (MCSM) [51–53], and no-core shell model (NCSM) [4, 10, 54–57] have been instrumental in providing a microscopic understanding of nuclear structure, clustering, and reaction dynamics in beryllium isotopes.

Comprehensive reviews have highlighted the importance of clustering phenomena in light nuclei and their impact on nuclear structure, reaction dynamics, and astrophysics [58–62]. These works emphasize the coexistence of cluster and shell-model features in neutron-rich isotopes and discuss the challenges in fully understanding the underlying mechanisms. The interplay between clustering and single-particle degrees of freedom remains a central theme in contemporary nuclear physics research.

While these theoretical methods have significantly advanced our understanding, a systematic *ab initio* study encompassing energies, radii, electromagnetic properties, and geometric structures across the beryllium isotopes is still lacking. Recent advancements in nuclear lattice effective field theory (NLEFT) offer promising avenues for such comprehensive investigations. The introduction of wavefunction matching techniques within NLEFT, combined with state-of-the-art next-to-next-to-next-to-leading order ($N^3\text{LO}$) chiral interactions, has led to remarkable agreement with experimental data across a range of nuclei, from the deuteron to medium-mass systems like ${}^{58}\text{Ni}$ [63]. Notably, NLEFT has successfully described the structure of the Hoyle state in ${}^{12}\text{C}$ [64, 65], α - α scattering processes [66], geometric configurations of the ${}^{12}\text{C}$ spectrum [67], nuclear thermodynamics [68], clustering in hot dilute matter [69], structure factors for hot neutron matter [70], hyper-neutron matter [71], and hypernuclei [72].

In this work, we present a systematic *ab initio* study of the p -shell beryllium isotopes using NLEFT with the $N^3\text{LO}$ in-

teraction. By employing wavefunction matching, we accurately calculate energies, radii, and electromagnetic properties, and explore the geometric structures of these isotopes. Our study addresses the emergent phenomena of clustering and halo structures along the beryllium isotope chain within a unified framework, providing new insights into their underlying nuclear dynamics and contributing to the broader understanding of clustering effects in light nuclei.

FORMALISM

We use the wavefunction matching method [63] to mitigate the Monte Carlo sign problem associated with high-fidelity $N^3\text{LO}$ chiral interactions. This method unitarily transforms the original Hamiltonian, H , into a new high-fidelity Hamiltonian, H' , such that its wave functions match those of a computationally simple Hamiltonian, H^S , up to a given radius. This transformation ensures that the expansion in powers of the difference $H' - H^S$ converges rapidly, allowing all higher-order corrections to be efficiently computed within first-order perturbation theory. For more details of the interaction, see Ref. [63]. For comparison, we also employ a simple $\text{SU}(4)$ -symmetric interaction, which was successfully used in earlier studies and fitted to reproduce the ground-state properties of ${}^4\text{He}$ and ${}^{12}\text{C}$ [67].

In the NLEFT framework, observables are calculated as

$$\langle O \rangle = \lim_{\tau \rightarrow \infty} \frac{\langle \Psi_0 | M^{L_t/2} O M^{L_t/2} | \Psi_0 \rangle}{\langle \Psi_0 | M^{L_t} | \Psi_0 \rangle}, \quad (1)$$

where Ψ_0 is the initial wave function, which is a Slater determinant of A -nucleon wave functions on the lattice, M is the normal-ordered transfer matrix operator: $e^{-H^S a_t}$: with temporal lattice spacing a_t , and L_t is the total number of lattice steps in the temporal direction. The Euclidean time τ is defined as the product $\tau = a_t \times L_t$. In our calculations we perform auxiliary-field Monte Carlo simulations, where using a Hubbard-Stratonovich transformation and auxiliary fields are introduced to decouple the particle densities, allowing them to couple directly to the auxiliary fields [73, 74].

To study the nuclear geometrical properties, we employ the pinhole algorithm [75] and its perturbative extension [76]. The method samples the positions of A -nucleons, denoted as \mathbf{n}_i , on the lattice (spin and isospin indices have been omitted) according to the following amplitude

$$Z = \langle \Psi_0 | M^{L_t/2} \rho(\mathbf{n}_1, \mathbf{n}_2, \dots, \mathbf{n}_A) M^{L_t/2} | \Psi_0 \rangle, \quad (2)$$

where $\rho(\mathbf{n}_1, \mathbf{n}_2, \dots, \mathbf{n}_A)$ is the normal-ordered product of single-nucleon density operators $\rho(\mathbf{n}_i) = a_i^\dagger(\mathbf{n}_i) a_i(\mathbf{n}_i)$. Let N_{pin} represent the total number of sampled pinhole configurations. These configurations can be written as

$$\left\{ \mathbf{N}^{(k)} = \left(\mathbf{n}_1^{(k)}, \mathbf{n}_2^{(k)}, \dots, \mathbf{n}_A^{(k)} \right) \right\}_{k=1}^{N_{\text{pin}}}. \quad (3)$$

where N_{pin} typically reaches several millions for the current study of beryllium isotopes. Each configuration then can be

transformed into the A -nucleon center-of-mass (c.m.) coordinate, \mathbf{r}_i , [75]:

$$\left\{ \mathbf{R}^{(k)} = \left(\mathbf{r}_1^{(k)}, \mathbf{r}_2^{(k)}, \dots, \mathbf{r}_A^{(k)} \right) \right\}_{k=1}^{N_{\text{pin}}}. \quad (4)$$

To account for the finite nucleon size (0.84fm) [77], a random Gaussian smearing is applied during the transformation from Eq. (3) to Eq. Eq. (4). This accounts for the proton size in the charge density distribution and further has the practical advantage of smoothing the density distribution [67].

The quadrupole moment for a given configuration can then be calculated as (the denominator required for normalization has been omitted)

$$\langle Q \rangle = e \sum_{k=1}^{N_{\text{pin}}} (-1)^{s_k} \sum_{i=1}^Z \left[r_i^{(k)} \right]^2 \left(3 \cos^2 \theta_i^{(k)} - 1 \right), \quad (5)$$

with $s_k = 0$ or 1 for the sign, and the summation is over protons. The reduced transition probability is

$$\langle B(E\lambda; I_1 \rightarrow I_2) \rangle = e^2 \sum_{\mu M_2} \left| \sum_{k=1}^{N_{\text{pin}}} (-1)^{s_k} \sum_{i=1}^Z r_i^\lambda Y_{\lambda\mu}(\hat{\mathbf{r}}_i) \right|^2. \quad (6)$$

The deformation parameters for a given pinhole configuration (k) are [78]

$$a_{20}^{(k)} = \frac{4\pi}{3AR_0^2} \sqrt{\frac{5}{16\pi}} \sum_{i=1}^A \left(3 \left[z_i^{(k)} \right]^2 - \left[r_i^{(k)} \right]^2 \right), \quad (7a)$$

$$a_{22}^{(k)} = \frac{4\pi}{3AR_0^2} \sqrt{\frac{15}{32\pi}} \sum_{i=1}^A \left(\left[x_i^{(k)} \right]^2 - \left[y_i^{(k)} \right]^2 + i x_i^{(k)} y_i^{(k)} \right), \quad (7b)$$

with $R_0 = 1.2 \text{ fm } A^{1/3}$. The Hill-Wheeler coordinates [79] β, γ can be calculated with:

$$a_{20}^{(k)} = \beta^{(k)} \cos \gamma^{(k)}, \quad a_{22}^{(k)} = \frac{1}{\sqrt{2}} \beta^{(k)} \sin \gamma^{(k)}. \quad (8)$$

By a suitable rotation, the expectation value of $\langle xy \rangle$ vanishes. The statistically average over N_{pin} configurations will give us a deformation distribution for a given state of nucleus. To distinguish it from single determinant deformation, we label it as β_{pin} and γ_{pin} .

Note that the expressions in Eqs. (4-7) have no explicit left $\langle L |$ and right $| R \rangle$ states information, they are encoded in Eq. (2). For transition observables (6) a multichannel calculation with different bra and ket states will be performed.

RESULTS AND DISCUSSION

The $N^3\text{LO}$ interaction described in Ref. [63] and $\text{SU}(4)$ -symmetric interaction in Ref. [67] are defined on lattices with spatial spacings $a = 1.32 \text{ fm}$ and 1.64 fm , respectively, which

correspond to momentum cutoffs $\Lambda = \pi/a \simeq 471$ MeV and 377 MeV. Additionally, the temporal lattice spacings for these interactions are defined as $a_t = 0.20$ fm and $a_t = 0.55$ fm, respectively, for these interactions. We perform our lattice calculation in a periodic cubic box with length $L = 10$ for the $N^3\text{LO}$ interaction and $L = 9$ for the $\text{SU}(4)$ -symmetric interaction (in lattice units), corresponding to $L = 13.2$ fm and 14.8 fm, respectively. The initial wave functions are constructed using shell-model wave functions, with the harmonic oscillator strength adjusted to achieve faster convergence. See Ref. [80] for the details on the configurations of the initial wave functions.

Fig. 1 displays the low-lying energy spectra of ${}^7\text{Be}$ to ${}^{12}\text{Be}$ calculated using NLEFT with the $N^3\text{LO}$ interaction, compared to experimental data [81–86]. The theoretical predictions show excellent agreement with experimental results, affirming the effectiveness of the $N^3\text{LO}$ interaction in accurately reproducing both ground and excited states of beryllium isotopes. As demonstrated in Ref. [63], NLEFT achieves high precision for ground state energies across a wide range of nuclei, and this precision extends to the excited states of beryllium isotopes. However, numerical challenges such as Euclidean time extrapolation and finite volume effects become more pronounced for excited states [80], making it more difficult to maintain the same level of accuracy as for ground states. Addressing these challenges will require further optimization of computational algorithms and fine-tuning of three-body forces. Despite these challenges, the successful application of NLEFT to beryllium isotopes underscores its potential for accurately capturing the complex dynamics of light nuclei.

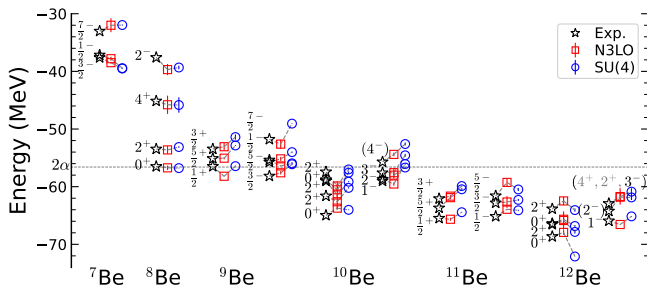


FIG. 1. Low-lying spectrum from ${}^7\text{Be}$ to ${}^{12}\text{Be}$ calculated by NLEFT using $N^3\text{LO}$ interaction [63] and $\text{SU}(4)$ interaction [67], compared to the data [81–86]. The error bars correspond to one standard deviation errors include stochastic errors and uncertainties in the Euclidean time extrapolation. The two α threshold is denoted by horizontal dashed line.

It is noteworthy that the simple $\text{SU}(4)$ -symmetric interaction [67], fitted to the ground states of ${}^4\text{He}$ and ${}^{12}\text{C}$, also provides an accurate description of most of the states, especially ${}^{11}\text{Be}$. The ground state of ${}^{11}\text{Be}$ has long posed a challenge to nuclear structure theory due to its inverted parity ordering, where the $1/2^+$ state lies below the $1/2^-$ state, contrary to shell-model predictions [4, 57, 61]. Using only

TABLE I. Energies of states in ${}^7\text{Be}$ and ${}^{10}\text{Be}$ calculated by NLEFT that have not been identified by experiments. For ${}^7\text{Be}$ some results from NCSM calculations [51] are listed for comparison.

	NLEFT, $N^3\text{LO}$	NLEFT, $\text{SU}(4)$	NCSM
${}^7\text{Be}, (3/2^+)$	-30.5(8)	-29.9(3)	-24.7
${}^7\text{Be}, (1/2^+)$	-28.8(1)	-31.9(2)	-27.8
${}^7\text{Be}, (5/2^+)$	-26.5(7)	-26.5(1)	
${}^{10}\text{Be}, A_1^+(3)$	-56.1(7)	-58.4(9)	

the $\text{SU}(4)$ -symmetric interaction, we successfully reproduce this ordering with high precision: $E(1/2^+) = -64.6(1)$ MeV and $E(1/2^-) = -64.1(1)$ MeV, compared to the experimental values of -65.5 MeV and -65.2 MeV, respectively. This result underscores the importance of many-body correlations in achieving accurate nuclear structure descriptions. The slight deviations between the $\text{SU}(4)$ results and experimental data indicate the breaking of $\text{SU}(4)$ symmetry in the nuclear interaction, as exemplified by ${}^{12}\text{Be}$, where neutrons fully occupy the $1p$ shell, unlike ${}^{12}\text{C}$, which primarily occupies the $1p_{3/2}$ shell. Future studies using $\text{SU}(4)$ -symmetric interaction will explore additional effects, such as the tensor force [87] or spin-orbit force [88], to further refine these calculations.

By exploring various configurations, we identify states in beryllium isotopes that have not yet been observed experimentally, as listed in Table I. The existence of positive-parity states in ${}^7\text{Be}$ has been a subject of long-standing debate [89–94]. Using shell-model wave functions with one proton excited to the sd shell, our calculations yield lower energies compared to the NCSM results [51].

For ${}^{10}\text{Be}$, a three-channel 0^+ calculation with *irrep* A_1^+ projection [95] reveals that the ground state is a mixture of $1p_{3/2}$ and $1p_{1/2}$ channels, the second 0^+ state is predominantly $2s_{1/2}$, and the third state also comprises a mixture of $1p_{3/2}$ and $1p_{1/2}$. While the 0_2^+ state with sd -shell or σ orbit characteristics is well established [39, 60], the nature of the third A_1^+ state remains unclear. Although it could correspond to a 4^+ state, its calculated energy ($-56 \sim -58$ MeV) is significantly lower than the experimental 4_1^+ at -53.2 MeV and the -49 MeV obtained from similar $J_z = 4$ calculations.

Fig. 2 displays the charge radii and point matter radii of beryllium isotopes with available experimental data [18, 96–98]. Our theoretical results, compared to calculations from AMD [14], FMD [18], and THSR [21–23], agree with experimental values within approximately 6% and follow the same trend. Notably, the halo structure of ${}^{11}\text{Be}$ is accurately reproduced using the $N^3\text{LO}$ interaction. In our framework, one of the valence neutron occupies a σ orbital, initiated from a shell-model wave function with the neutron placed in the sd shell. As the Euclidean projection time increases, the $1/2^+$ ground state emerges, positioned below the ${}^{10}\text{Be} + n$ threshold, thereby forming a bound halo nucleus. This extended σ orbital results in significant spatial extension, consider those with only 1 neutron occupation, for positive-parity states in

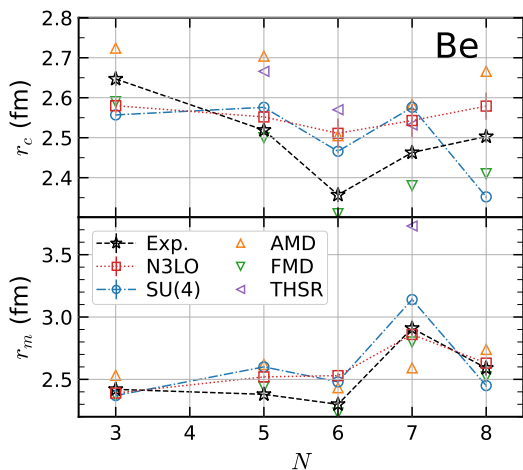


FIG. 2. Radii from ${}^7\text{Be}$ to ${}^{12}\text{Be}$ calculated by NLEFT using N^3LO interaction [63] and $\text{SU}(4)$ interaction [67], compared to the data [18, 96–98] and other theoretical calculations [14, 18, 21–23]. For Refs. [14, 21, 23] proton size, neutron size, and relativistic correction are added. (Upper panel) charge radii; (lower panel) point matter radii. The error bars correspond to one standard deviation errors include stochastic errors and uncertainties in the Euclidean time extrapolation.

TABLE II. The quadrupole moment and transition rates of Be isotopes calculated by NLEFT using the N^3LO interaction [63] and $\text{SU}(4)$ interaction [67], in comparison with experiment. Units for Q and $m(E0)$ are efm^2 , for $B(E1)$ are e^2fm^2 , and for $B(E2)$ are e^2fm^4 .

	SU(4)	N^3LO	Exp.
${}^7\text{Be}$ $E2, \frac{3}{2}^- \rightarrow \frac{1}{2}^-$	16.0(2)	15.2(5)	26(6)(3) [99]
${}^9\text{Be}$ $Q(\frac{3}{2}^-)$	7.3(1)	7.4(1.0)	5.29(4) [100]
$E1, \frac{1}{2}^+ \rightarrow \frac{3}{2}^-$	0.131(3)	0.060(15)	0.136(2) [101]
$E1, \frac{5}{2}^+ \rightarrow \frac{3}{2}^-$	0.045(14)	0.049(5)	0.010(8) [85]
$E2, \frac{5}{2}^- \rightarrow \frac{3}{2}^-$	35.7(1.8)	27.8(1.9)	27.1(2.0) [85]
$E2, \frac{7}{2}^- \rightarrow \frac{3}{2}^-$	11.6(2.5)	5.3(8)	9.5(4.1) [85]
${}^{10}\text{Be}$ $E1, 3_1^- \rightarrow 2_1^+$	0.026(2)	0.004(3)	0.009(1) [85]
$E2, 2_1^+ \rightarrow 0_1^+$	10.6(4)	8.5(9)	9.2(3) [46]
${}^{11}\text{Be}$ $E1, \frac{1}{2}^- \rightarrow \frac{1}{2}^+$	0.023(3)	0.038(3)	0.102(2) [102]
${}^{12}\text{Be}$ $E1, 0_1^+ \rightarrow 1_1^-$	0.049(2)	0.056(26)	0.051(13) [103]
$E2, 2_1^+ \rightarrow 0_1^+$	7.8(1.1)	9.0(3.1)	14.2(1.0)(2.0) [6]

${}^7\text{Be}$, ${}^9\text{Be}$, and ${}^{11}\text{Be}$, as well as for negative-parity states in ${}^8\text{Be}$, ${}^{10}\text{Be}$, and ${}^{12}\text{Be}$. These findings highlight the strong clustering and halo characteristics inherent to beryllium isotopes.

We present the calculated quadrupole moments and transition rates for ${}^7\text{Be}$ to ${}^{12}\text{Be}$ in Table II. These transition calculations are challenging due to slow convergence in Euclidean time and complex multichannel dynamics [104]. To address this, we employed extended Euclidean time projections and applied extrapolation techniques, see [80]. Our results generally agree with the experimental data, with deviations observed in some cases. Given that electromagnetic observables are highly sensitive to nuclear geometric structures, achieving

precise reproduction is inherently ambitious. Nonetheless, our systematic and parameter-free approach provides valuable insights for refining nuclear forces on the lattice, particularly concerning three-body interactions.

Numerous theoretical studies have investigated these electromagnetic properties [4, 11–13, 15, 18, 19, 28–31, 33, 45–48, 51, 53, 56, 57, 105], which we compare in [80]. Additionally, we are developing a new method that combines second-order perturbative Monte Carlo [106] with a trimmed sampling algorithm [107] to study transitions involving second 0^+ and 2^+ states using the N^3LO interaction. Details of this technique and its results will be presented in an upcoming publication.

Next we would like to turn to the study of intrinsic shape. Recent experimental advancements, such as the collective-flow-assisted nuclear shape-imaging method introduced by STAR [108], have provided unprecedented insights into the shapes of atomic nuclei by capturing collision-specific snapshots of their spatial matter distributions. These exciting developments underscore the importance of complementary theoretical approaches.

In Fig. 3, we present the probability distributions of the deformation parameters β_{pin} and γ_{pin} for the beryllium isotopes, obtained through sampling pinhole configurations that incorporate all many-body correlations. This model-independent analysis statistically represents the relative positions of all nucleons, distinguishing it from traditional energy surface plots based on single Slater determinants.

Our results reveal that the occupation of different neutron orbitals, π or σ orbitals (or p or sd shells in the shell model picture), dramatically alters the nuclear shape. Specifically, valence neutrons in σ orbitals induce more prolate deformations, whereas occupation of the π orbital leads to more spherical shapes. These shape transitions are more pronounced in lighter isotopes and diminish with increasing mass number. For ${}^7\text{Be}$ and ${}^8\text{Be}$, which lack valence neutrons, parity changes arise from breaking a particle within the cluster, resulting in higher excitation energies and more substantial shape modifications. Notably, the unconfirmed $3/2^+$ state in ${}^7\text{Be}$ exhibits a broad distribution in the $\beta_{\text{pin}}-\gamma_{\text{pin}}$ plane, indicating significant shape variability.

These findings align well with the nuclear molecular framework and highlight the strong clustering and halo characteristics inherent to beryllium isotopes. Our model-independent approach complements experimental shape-imaging techniques, providing a comprehensive understanding of nuclear geometry from an *ab initio* perspective.

Finally, we present intrinsic density plots of selected states in beryllium isotopes in Fig. 4. To obtain these intrinsic densities, we adopt the strategy from Ref. [67], which groups the closest two protons and two neutrons and randomly aligns the clusters along the $\pm z$ -axis. This method ensures a balanced representation of nuclear shapes, avoiding the overemphasis of any single axis that occurs when aligning configurations based on the principal axis [49].

Panels (a)–(d) display the total density for ${}^8\text{Be}$, ${}^{10}\text{Be}$, and

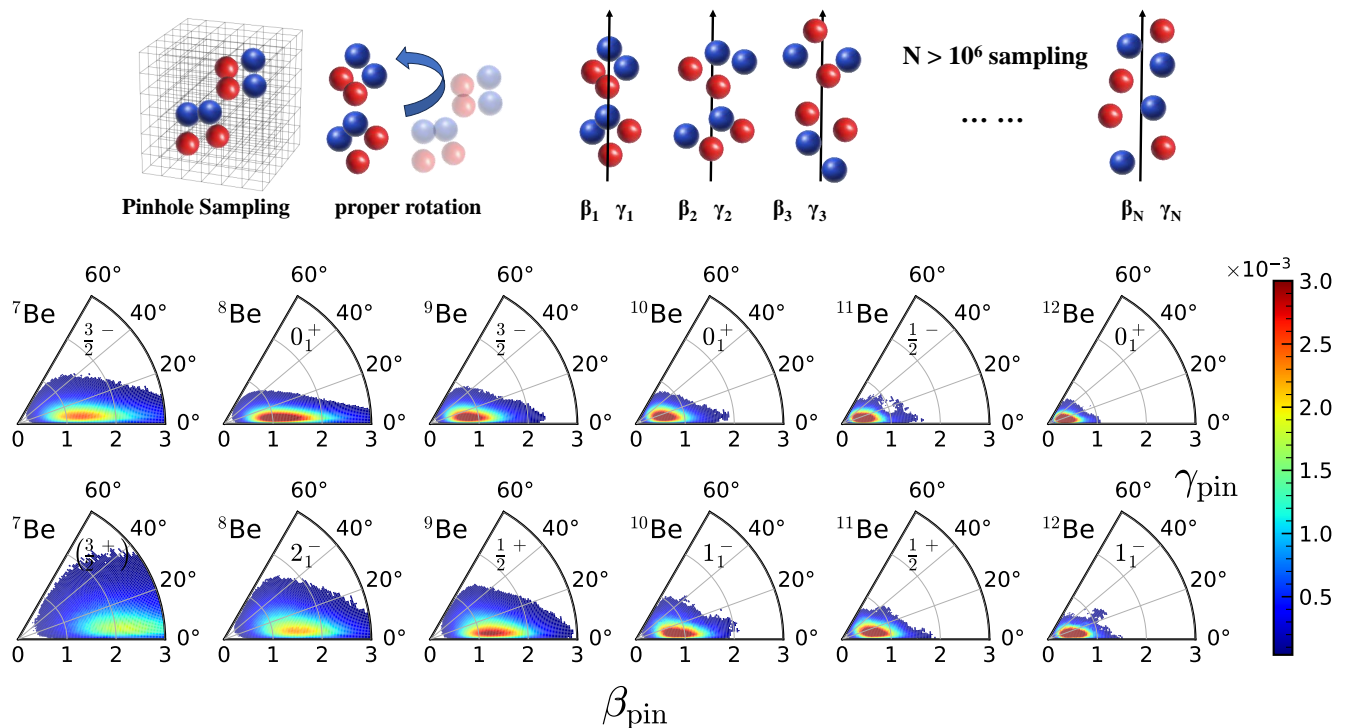


FIG. 3. Probability distribution of the deformation parameter β_{pin} and γ_{pin} in Eq. (8) through sampling of pinhole configuration by NLEFT using $N^3\text{LO}$ interaction, with red color represent a higher probability and blue color lower. The third component of total spin is fixed at $J_z = J$.

^{11}Be ($1/2^-$ and $1/2^+$ states). ^8Be clearly shows a strong two-alpha cluster structure as expected. Adding valence neutrons in ^{10}Be and ^{11}Be slightly diminishes the cluster formation while enhancing the neck region between clusters. Comparing the $1/2^-$ and $1/2^+$ states of ^{11}Be , we observe significantly different shapes: the π orbital occupation results in a more rounded nucleus, whereas the σ orbital induces a pronounced prolate deformation, consistent with nuclear molecular dynamics in other studies [39, 44, 52, 109].

Panels (e)–(h) illustrate the valence neutron densities, scaled by a constant factor of 5 or by r^2 . In panel (e), the π orbital in ^{11}Be naturally emerges from the $N^3\text{LO}$ interaction, displaying a distinct distribution. For the $1/2^+$ state in panel (f), one neutron occupies the σ orbital, reducing the π orbital density. Applying an r^2 scaling in panels (g) and (h) reveals the large spatial extension of the last neutron in the $1/2^+$ state, characteristic of a halo nucleus. This extended distribution aligns with other models [16, 39], showing enhanced density around $r \sim 0$ and along the $\pm z$ -axis, alongside shell-model sd characteristics indicative of a halo structure. Due to lower statistics, there is a larger fluctuation in the valence neutron distribution.

Overall, from ^8Be to ^{12}Be , the ground-state shapes transition from pronounced two-center clusters to more rounded (or prolate configurations in the special case of ^{11}Be). Notably, ^{11}Be uniquely exhibits a prolate halo structure due to σ

orbital occupation. These intrinsic density analyses, derived from our *ab initio* NLEFT framework, provide a comprehensive understanding of the geometric evolution and clustering phenomena in beryllium isotopes.

SUMMARY AND DISCUSSION

We have systematically studied the p -shell beryllium isotopes using nuclear lattice effective field theory (NLEFT) with both the $N^3\text{LO}$ interaction [63] and a simple $\text{SU}(4)$ -symmetric interaction [67]. Our calculations for the low-lying spectra, radii, and electromagnetic observables show good agreement with experimental data. Notably, the $\text{SU}(4)$ -symmetric interaction, fitted only to the ground states of ^4He and ^{12}C , successfully reproduces the correct ordering of the $\frac{1}{2}^+$ ground state in ^{11}Be , highlighting the importance of many-body correlations. We also investigate the halo structure of ^{11}Be , the geometric differences between negative- and positive-parity states, and intrinsic density distributions. The debated positive-parity states in ^7Be are obtained by initializing with one proton excited to the sd shell, resulting in highly deformed and mixed configurations. Adding valence neutrons diminishes the two- α cluster structure while strengthening the neck region. Transitioning from natural-parity (π orbital) to unnatural-parity (σ orbital) states induces more prolate and

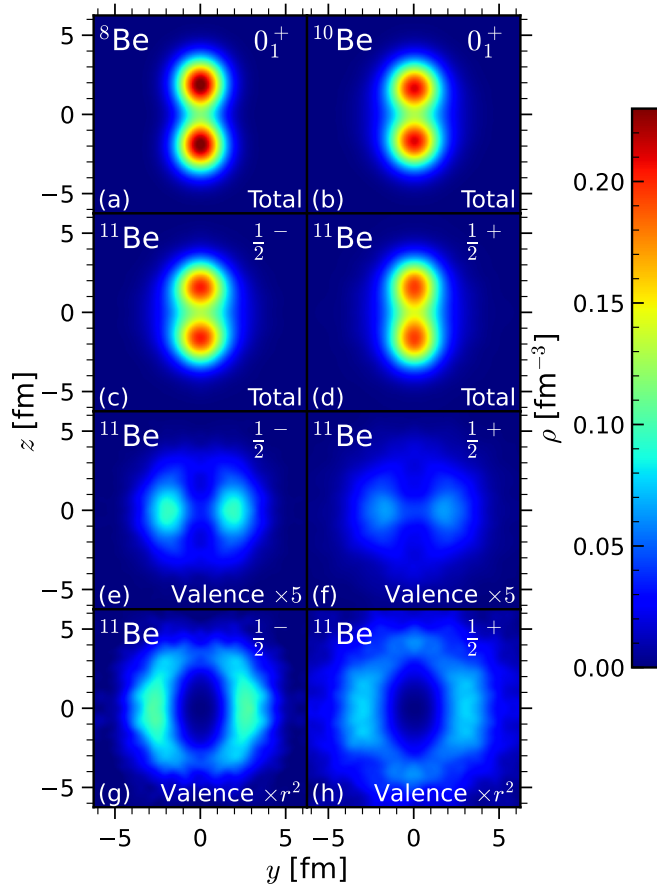


FIG. 4. Intrinsic density at $x = 0$ plane of selected states of beryllium isotopes obtained by NLEFT using N^3LO interaction. The third component of total spin is fixed at $J_z = J$.

triaxially deformed shapes.

These findings demonstrate the efficiency of NLEFT combined with our shape quantification technique in capturing the intricate dynamics of light nuclei, providing new insights into clustering and halo phenomena in neutron-rich systems. This work advances the understanding of nuclear structure in exotic isotopes and highlights the potential of unified *ab initio* approaches in elucidating complex nuclear behaviors. Further detailed analyses of intrinsic structures are underway.

ACKNOWLEDGMENTS

We are grateful for discussions with Jie Meng and the members of the NLEFT Collaboration. This work is supported in part by the European Research Council (ERC) under the European Union's Horizon 2020 research and innovation programme (ERC AdG EXOTIC, grant agreement No. 101018170), by DFG and NSFC through funds provided to the Sino-German CRC 110 "Symmetries and the Emergence of Structure in QCD" (NSFC Grant No. 11621131001, DFG

Grant No. TRR110). The work of UGM was supported in by the CAS President's International Fellowship Initiative (PIFI) (Grant No. 2025PD0022). The work of SE is supported in part by the Scientific and Technological Research Council of Turkey (TUBITAK project no. 120F341). The work of DL is supported in part by the U.S. Department of Energy (Grant Nos. DE-SC0013365, DE-SC0023658, DE-SC0024586, PHY-2310620) and the Nuclear Computational Low-Energy Initiative (NUCLEI) SciDAC project. The authors gratefully acknowledge the Gauss Centre for Supercomputing e.V. (www.gauss-centre.eu) for funding this project by providing computing time on the GCS Supercomputer JUWELS at Jülich Supercomputing Centre (JSC).

* meissner@hiskp.uni-bonn.de

- [1] E. G. Adelberger, S. M. Austin, J. N. Bahcall, A. B. Balantekin, G. Bogaert, L. S. Brown, L. Buchmann, F. E. Cecil, A. E. Champagne and L. de Braekeleer, *et al.* Rev. Mod. Phys. **70** (1998), 1265-1292 doi:10.1103/RevModPhys.70.1265 [arXiv:astro-ph/9805121 [astro-ph]].
- [2] E. G. Adelberger, A. B. Balantekin, D. Bemmerer, C. A. Bertulani, J. W. Chen, H. Costantini, M. Couder, R. Cyburt, B. Davids and S. J. Freedman, *et al.* Rev. Mod. Phys. **83** (2011), 195 doi:10.1103/RevModPhys.83.195 [arXiv:1004.2318 [nucl-ex]].
- [3] P. J. Li, D. Beaumel, J. Lee, M. Assié, S. Chen, S. Franchoo, J. Gibelin, F. Hammache, T. Harada and Y. Kanada-En'yo, *et al.* Phys. Rev. Lett. **131** (2023) no.21, 212501 doi:10.1103/PhysRevLett.131.212501 [arXiv:2311.13129 [nucl-ex]].
- [4] A. Calci, P. Navrátil, R. Roth, J. Dohet-Eraly, S. Quaglioni and G. Hupin, Phys. Rev. Lett. **117** (2016) no.24, 242501 doi:10.1103/PhysRevLett.117.242501 [arXiv:1608.03318 [nucl-th]].
- [5] I. Talmi and I. Unna, Phys. Rev. Lett. **4** (1960), 469-470 doi:10.1103/PhysRevLett.4.469
- [6] C. Morse, E. A. McCutchan, H. Iwasaki, C. J. Lister, V. M. Bader, D. Bazin, S. Beceiro Novo, P. Chowdhury, A. Gade and T. D. Johnson, *et al.* Phys. Lett. B **780** (2018), 227-232 doi:10.1016/j.physletb.2018.03.004
- [7] J. Chen, J. L. Lou, Y. L. Ye, Z. H. Li, D. Y. Pang, C. X. Yuan, Y. C. Ge, Q. T. Li, H. Hua and D. X. Jiang, *et al.* Phys. Lett. B **781** (2018), 412-416 doi:10.1016/j.physletb.2018.04.016 [arXiv:1805.06074 [nucl-ex]].
- [8] S. D. Pain, W. N. Catford, N. A. Orr, J. C. Angeliq, N. I. Ashwood, V. Bouchat, N. M. Clarke, N. Curtis, M. Freer and B. R. Fulton, *et al.* Phys. Rev. Lett. **96** (2006), 032502 doi:10.1103/PhysRevLett.96.032502 [arXiv:nucl-ex/0510048 [nucl-ex]].
- [9] A. Navin, D. W. Anthony, T. Aumann, T. Baumann, D. Bazin, Y. Blumenfeld, B. A. Brown, T. Glasmacher, P. G. Hansen and R. W. Ibbotson, *et al.* Phys. Rev. Lett. **85** (2000), 266-269 doi:10.1103/PhysRevLett.85.266
- [10] P. Navrátil, V. G. Gueorguiev, J. P. Vary, W. E. Ormand and A. Nogga, Phys. Rev. Lett. **99** (2007), 042501 doi:10.1103/PhysRevLett.99.042501 [arXiv:nucl-th/0701038 [nucl-th]].
- [11] T. Myo, M. Lyu, Q. Zhao, M. Isaka, N. Wan, H. Takemoto and H. Horiuchi, Phys. Rev. C **108** (2023) no.6, 064314 doi:10.1103/PhysRevC.108.064314 [arXiv:2311.16391 [nucl-

- th]].
- [12] M. Dan, R. Chatterjee and M. Kimura, *Eur. Phys. J. A* **57** (2021) no.6, 203 doi:10.1140/epja/s10050-021-00526-4 [arXiv:2101.02885 [nucl-th]].
- [13] Y. Kanada-En'yo, *Phys. Rev. C* **93** (2016) no.2, 024322 doi:10.1103/PhysRevC.93.024322 [arXiv:1511.08530 [nucl-th]].
- [14] Y. Kanada-En'yo, *Phys. Rev. C* **91** (2015) no.1, 014315 doi:10.1103/PhysRevC.91.014315 [arXiv:1411.0765 [nucl-th]].
- [15] Y. Kanada-En'yo and H. Horiuchi, *Phys. Rev. C* **68** (2003), 014319 doi:10.1103/PhysRevC.68.014319 [arXiv:nucl-th/0301059 [nucl-th]].
- [16] Y. Kanada-En'yo and H. Horiuchi, *Phys. Rev. C* **66** (2002), 024305 doi:10.1103/PhysRevC.66.024305 [arXiv:nucl-th/0204041 [nucl-th]].
- [17] Y. Kanada-En'yo, H. Horiuchi and A. Dote, *Phys. Rev. C* **60** (1999), 064304 doi:10.1103/PhysRevC.60.064304 [arXiv:nucl-th/9905048 [nucl-th]].
- [18] A. Krieger, K. Blaum, M. L. Bissell, N. Frommgen, C. Geppert, M. Hammen, K. Kreim, M. Kowalska, J. Kramer and T. Neff, *et al. Phys. Rev. Lett.* **108** (2012), 142501 doi:10.1103/PhysRevLett.108.142501 [arXiv:1202.4873 [physics.atom-ph]].
- [19] N. Itagaki and S. Okabe, *Phys. Rev. C* **61** (2000), 044306 doi:10.1103/PhysRevC.61.044306
- [20] W. Von Oertzen, *Z. Phys. A* **354** (1996) 37–43 doi:10.1007/BF02903274
- [21] M. Lyu, Z. Ren, H. Horiuchi, B. Zhou, Y. Funaki, G. Röpke, P. Schuck, A. Tohsaki, C. Xu and T. Yamada, *Eur. Phys. J. A* **57** (2021) no.2, 51 doi:10.1140/epja/s10050-021-00363-5
- [22] M. Lyu, Z. Ren, B. Zhou, Y. Funaki, H. Horiuchi, G. Röpke, P. Schuck, A. Tohsaki, C. Xu and T. Yamada, *Phys. Rev. C* **93** (2016) no.5, 054308 doi:10.1103/PhysRevC.93.054308 [arXiv:1512.07727 [nucl-th]].
- [23] M. Lyu, Z. Ren, B. Zhou, Y. Funaki, H. Horiuchi, G. Röpke, P. Schuck, A. Tohsaki, C. Xu and T. Yamada, *Phys. Rev. C* **91** (2015) no.1, 014313 doi:10.1103/PhysRevC.91.014313 [arXiv:1408.5293 [nucl-th]].
- [24] Q. Zhao, M. Kimura, B. Zhou and S. h. Shin, *Phys. Rev. C* **106** (2022) no.5, 054313 doi:10.1103/PhysRevC.106.054313 [arXiv:2207.13366 [nucl-th]].
- [25] T. Fukui, *J. Phys. G* **49** (2022) no.5, 055102 doi:10.1088/1361-6471/ac58b3 [arXiv:2012.14217 [nucl-th]].
- [26] B. Zhou, M. Kimura, Q. Zhao and S. h. Shin, *Eur. Phys. J. A* **56** (2020) no.11, 298 doi:10.1140/epja/s10050-020-00306-6
- [27] S. Li, T. Myo, Q. Zhao, H. Toki, H. Horiuchi, C. Xu, J. Liu, M. Lyu and Z. Ren, *Phys. Rev. C* **101** (2020) no.6, 064307 doi:10.1103/PhysRevC.101.064307 [arXiv:2005.04409 [nucl-th]].
- [28] P. Descouvemont and N. Itagaki, *PTEP* **2020** (2020) no.2, 023D02 doi:10.1093/ptep/ptz169
- [29] V. Della Rocca and F. Iachello, *Nucl. Phys. A* **973** (2018), 1-32 doi:10.1016/j.nuclphysa.2018.02.003
- [30] M. Dufour, P. Descouvemont and F. Nowacki, *Nucl. Phys. A* **836** (2010), 242-255 doi:10.1016/j.nuclphysa.2010.02.002
- [31] C. Romero-Redondo, E. Garrido, D. V. Fedorov and A. S. Jensen, *Phys. Rev. C* **77** (2008), 054313 doi:10.1103/PhysRevC.77.054313 [arXiv:0804.2351 [nucl-th]].
- [32] M. Ito, N. Itagaki, H. Sakurai and K. Ikeda, *Phys. Rev. Lett.* **100** (2008), 182502 doi:10.1103/PhysRevLett.100.182502
- [33] K. Arai, P. Descouvemont, D. Baye and W. N. Catford, *Phys. Rev. C* **68** (2003), 014310 doi:10.1103/PhysRevC.68.014310
- [34] P. Descouvemont, *Nucl. Phys. A* **699** (2002), 463-478 doi:10.1016/S0375-9474(01)01286-6
- [35] P. Descouvemont, *Phys. Rev. C* **39** (1989), 1557-1562 doi:10.1103/PhysRevC.39.1557
- [36] B. Zhou, Y. Funaki, H. Horiuchi and A. Tohsaki, *Front. Phys. (Beijing)* **15** (2020) no.1, 14401 doi:10.1007/s11467-019-0917-0 [arXiv:1905.00788 [nucl-th]].
- [37] M. Kimura, T. Suhara and Y. Kanada-En'yo, *Eur. Phys. J. A* **52** (2016) no.12, 373 doi:10.1140/epja/i2016-16373-9 [arXiv:1612.09432 [nucl-th]].
- [38] Y. Funaki, H. Horiuchi and A. Tohsaki, *Prog. Part. Nucl. Phys.* **82** (2015), 78-132 doi:10.1016/j.pnpnp.2015.01.001
- [39] W. von Oertzen, M. Freer, and Y. Kanada-En'yō, *Phys. Rep.* **432**, no. 2 (2006) 43–113 doi:10.1016/j.physrep.2006.06.001
- [40] J. Geng, P. W. Zhao, Y. F. Niu and W. H. Long, *Phys. Lett. B* **858** (2024), 139036 doi:10.1016/j.physletb.2024.139036
- [41] J. Geng, Y. F. Niu and W. H. Long, *Chin. Phys. C* **47** (2023) no.4, 044102 doi:10.1088/1674-1137/acb7cd [arXiv:2303.04987 [nucl-th]].
- [42] J. P. Ebran, E. Khan, T. Niksic and D. Vretenar, *Phys. Rev. C* **90** (2014) no.5, 054329 doi:10.1103/PhysRevC.90.054329 [arXiv:1406.2473 [nucl-th]].
- [43] J. P. Linares Fernandez, N. Michel, M. Płoszajczak and A. Mercenne, *Phys. Rev. C* **108** (2023) no.4, 044616 doi:10.1103/PhysRevC.108.044616 [arXiv:2306.05215 [nucl-th]].
- [44] J. Carlson, S. Gandolfi, F. Pederiva, S. C. Pieper, R. Schiavilla, K. E. Schmidt and R. B. Wiringa, *Rev. Mod. Phys.* **87** (2015), 1067 doi:10.1103/RevModPhys.87.1067 [arXiv:1412.3081 [nucl-th]].
- [45] S. Pastore, S. C. Pieper, R. Schiavilla and R. B. Wiringa, *Phys. Rev. C* **87** (2013) no.3, 035503 doi:10.1103/PhysRevC.87.035503 [arXiv:1212.3375 [nucl-th]].
- [46] E. A. McCutchan, C. J. Lister, R. B. Wiringa, S. C. Pieper, D. Seweryniak, J. P. Greene, M. P. Carpenter, C. J. Chiara, R. V. F. Janssens and T. L. Khoo, *et al. Phys. Rev. Lett.* **103** (2009), 192501 doi:10.1103/PhysRevLett.103.192501 [arXiv:0907.3688 [nucl-ex]].
- [47] M. Pervin, S. C. Pieper and R. B. Wiringa, *Phys. Rev. C* **76** (2007), 064319 doi:10.1103/PhysRevC.76.064319 [arXiv:0710.1265 [nucl-th]].
- [48] S. C. Pieper, K. Varga and R. B. Wiringa, *Phys. Rev. C* **66** (2002), 044310 doi:10.1103/PhysRevC.66.044310 [arXiv:nucl-th/0206061 [nucl-th]].
- [49] R. B. Wiringa, S. C. Pieper, J. Carlson and V. R. Pandharipande, *Phys. Rev. C* **62** (2000), 014001 doi:10.1103/PhysRevC.62.014001 [arXiv:nucl-th/0002022 [nucl-th]].
- [50] K. Kravvaris and A. Volya, *Phys. Rev. Lett.* **119** (2017) no.6, 062501 doi:10.1103/PhysRevLett.119.062501
- [51] M. Vorabbi, P. Navrátil, S. Quaglioni and G. Hupin, *Phys. Rev. C* **100** (2019) no.2, 024304 doi:10.1103/PhysRevC.100.024304 [arXiv:1906.09258 [nucl-th]].
- [52] T. Yoshida, N. Shimizu, T. Abe and T. Otsuka, *Few Body Syst.* **54** (2013) no.7-10, 1465-1468 doi:10.1007/s00601-013-0680-7
- [53] L. Liu, T. Otsuka, N. Shimizu, Y. Utsuno and R. Roth, *Phys. Rev. C* **86** (2012), 014302 doi:10.1103/PhysRevC.86.014302 [arXiv:1105.2983 [nucl-th]].
- [54] A. E. McCoy, M. A. Caprio, P. Maris and P. J. Fasano, *Phys. Lett. B* **856** (2024), 138870 doi:10.1016/j.physletb.2024.138870 [arXiv:2402.12606 [nucl-th]].
- [55] M. A. Caprio, A. E. McCoy, P. J. Fasano and T. Dytrych, *Bulg. J. Phys.* **49** (2022) no.1, 057-066

- doi:10.55318/bgjp.2022.49.1.057 [arXiv:2112.04056 [nucl-th]].
- [56] T. Heng, J. P. Vary and P. Maris, *Phys. Rev. C* **95** (2017) no.1, 014306 doi:10.1103/PhysRevC.95.014306 [arXiv:1602.00156 [nucl-th]].
- [57] C. Forssen, P. Navratil, W. E. Ormand and E. Caurier, *Phys. Rev. C* **71** (2005), 044312 doi:10.1103/PhysRevC.71.044312 [arXiv:nucl-th/0412049 [nucl-th]].
- [58] I. Lombardo and D. Dell'Aquila, *Riv. Nuovo Cim.* **46** (2023) no.9, 521-618 doi:10.1007/s40766-023-00047-4
- [59] B. Gnoffo, S. Pirrone, G. Politi, G. Cardella, E. De Filippo, E. Geraci, C. Maiolino, N. S. Martorana, A. Pagano, E. V. Pagano, and others, *Front. Phys.* **10** (2022) 1061633 doi:10.3389/fphy.2022.1061633
- [60] Y. Kanada-En'yo and H. Horiuchi, *Front. Phys. (Beijing)* **13** (2018) no.6, 132108 doi:10.1007/s11467-018-0830-y
- [61] H. T. Fortune, *Eur. Phys. J. A* **54** (2018) no.3, 51 doi:10.1140/epja/i2018-12489-2
- [62] M. Freer, H. Horiuchi, Y. Kanada-En'yo, D. Lee and U. G. Meißner, *Rev. Mod. Phys.* **90** (2018) no.3, 035004 doi:10.1103/RevModPhys.90.035004 [arXiv:1705.06192 [nucl-th]].
- [63] S. Elhatisari, L. Bovermann, Y. Z. Ma, E. Epelbaum, D. Frame, F. Hildenbrand, M. Kim, Y. Kim, H. Krebs and T. A. Lähde, *et al. Nature* **630** (2024) no.8015, 59-63 doi:10.1038/s41586-024-07422-z [arXiv:2210.17488 [nucl-th]].
- [64] E. Epelbaum, H. Krebs, D. Lee and U.-G. Meissner, *Phys. Rev. Lett.* **106** (2011), 192501 doi:10.1103/PhysRevLett.106.192501 [arXiv:1101.2547 [nucl-th]].
- [65] E. Epelbaum, H. Krebs, T. A. Lähde, D. Lee and U.-G. Meissner, *Phys. Rev. Lett.* **109** (2012), 252501 doi:10.1103/PhysRevLett.109.252501 [arXiv:1208.1328 [nucl-th]].
- [66] S. Elhatisari, D. Lee, G. Rupak, E. Epelbaum, H. Krebs, T. A. Lähde, T. Luu and U.-G. Meißner, *Nature* **528** (2015), 111 doi:10.1038/nature16067 [arXiv:1506.03513 [nucl-th]].
- [67] S. Shen, S. Elhatisari, T. A. Lähde, D. Lee, B. N. Lu and U.-G. Meißner, *Nature Commun.* **14** (2023) no.1, 2777 doi:10.1038/s41467-023-38391-y [arXiv:2202.13596 [nucl-th]].
- [68] B. N. Lu, N. Li, S. Elhatisari, D. Lee, J. E. Drut, T. A. Lähde, E. Epelbaum and U.-G. Meißner, *Phys. Rev. Lett.* **125** (2020) no.19, 192502 doi:10.1103/PhysRevLett.125.192502 [arXiv:1912.05105 [nucl-th]].
- [69] Z. Ren, S. Elhatisari, T. A. Lähde, D. Lee and U.-G. Meißner, *Phys. Lett. B* **850** (2024), 138463 doi:10.1016/j.physletb.2024.138463 [arXiv:2305.15037 [nucl-th]].
- [70] Y. Z. Ma, Z. Lin, B. N. Lu, S. Elhatisari, D. Lee, N. Li, U.-G. Meißner, A. W. Steiner and Q. Wang, *Phys. Rev. Lett.* **132** (2024) no.23, 232502 doi:10.1103/PhysRevLett.132.232502 [arXiv:2306.04500 [nucl-th]].
- [71] H. Tong, S. Elhatisari and U.-G. Meißner, [arXiv:2405.01887 [nucl-th]].
- [72] F. Hildenbrand, S. Elhatisari, Z. Ren and U.-G. Meißner, *Eur. Phys. J. A* **60** (2024) no.10, 215 doi:10.1140/epja/s10050-024-01427-y [arXiv:2406.17638 [nucl-th]].
- [73] D. Lee, *Prog. Part. Nucl. Phys.* **63** (2009), 117-154 [arXiv:0804.3501 [nucl-th]].
- [74] T. A. Lähde and U.-G. Meißner, *Lect. Notes Phys.* **957** (2019), 1-396 Springer, 2019, ISBN 978-3-030-14187-5, 978-3-030-14189-9
- [75] S. Elhatisari, E. Epelbaum, H. Krebs, T. A. Lähde, D. Lee, N. Li, B. N. Lu, U.-G. Meißner and G. Rupak, *Phys. Rev. Lett.* **119** (2017) no.22, 222505 [arXiv:1702.05177 [nucl-th]].
- [76] B. N. Lu, N. Li, S. Elhatisari, D. Lee, E. Epelbaum and U. G. Meißner, *Phys. Lett. B* **797**, 134863 (2019) doi:10.1016/j.physletb.2019.134863 [arXiv:1812.10928 [nucl-th]].
- [77] Y. H. Lin, H. W. Hammer and U.-G. Meißner, *Phys. Rev. Lett.* **128** (2022) no.5, 052002 [arXiv:2109.12961 [hep-ph]].
- [78] P. Ring and P. Schuck, *The Nuclear Many-Body Problem*, Springer Science & Business Media, 2004.
- [79] D. L. Hill and J. A. Wheeler, *Phys. Rev.* **89** (1953), 1102-1145 doi:10.1103/PhysRev.89.1102
- [80] see the *Supplemental Material*
- [81] W. Liu, J. L. Lou, Y. L. Ye, S. M. Wang, Z. W. Tan, Z. H. Li, Q. T. Li, H. Hua, X. F. Yang and J. Y. Xu, *et al. Phys. Rev. C* **105** (2022) no.3, 034613 doi:10.1103/PhysRevC.105.034613
- [82] M. Wang, W. J. Huang, F. G. Kondev, G. Audi and S. Naimi, *Chin. Phys. C* **45** (2021) no.3, 030003 doi:10.1088/1674-1137/abddaf
- [83] J. H. Kelley, J. E. Purcell and C. G. Sheu, *Nucl. Phys. A* **968** (2017), 71-253 doi:10.1016/j.nuclphysa.2017.07.015
- [84] J. H. Kelley, E. Kwan, J. E. Purcell, C. G. Sheu and H. R. Weller, *Nucl. Phys. A* **880** (2012), 88-195 doi:10.1016/j.nuclphysa.2012.01.010
- [85] D. R. Tilley, J. H. Kelley, J. L. Godwin, D. J. Millener, J. E. Purcell, C. G. Sheu and H. R. Weller, *Nucl. Phys. A* **745** (2004), 155-362 doi:10.1016/j.nuclphysa.2004.09.059
- [86] D. R. Tilley, C. M. Cheves, J. L. Godwin, G. M. Hale, H. M. Hofmann, J. H. Kelley, C. G. Sheu and H. R. Weller, *Nucl. Phys. A* **708** (2002), 3-163 doi:10.1016/S0375-9474(02)00597-3
- [87] T. Otsuka, T. Suzuki, R. Fujimoto, H. Grawe and Y. Akaishi, *Phys. Rev. Lett.* **95** (2005), 232502 doi:10.1103/PhysRevLett.95.232502
- [88] Z. Niu and B. Lu, in preparation
- [89] D. Piatti, T. Chillery, R. Depalo, M. Aliotta, D. Bemmerer, A. Best, A. Boeltzig, C. Broggini, C. G. Bruno and A. Caciolli, *et al. Phys. Rev. C* **102** (2020) no.5, 052802 doi:10.1103/PhysRevC.102.052802
- [90] T. Szücs, G. G. Kiss, G. Gyürky, Z. Halász, T. N. Szegedi and Z. Fülöp, *Phys. Rev. C* **99** (2019) no.5, 055804 [erratum: *Phys. Rev. C* **105** (2022) no.6, 069901] doi:10.1103/PhysRevC.99.055804 [arXiv:1905.01711 [nucl-th]].
- [91] A. Gnech and L. E. Marcucci, *Nucl. Phys. A* **987** (2019), 1-15 doi:10.1016/j.nuclphysa.2019.04.005 [arXiv:1902.05881 [nucl-th]].
- [92] G. X. Dong, N. Michel, K. Fosse, M. Płoszajczak, Y. Jagannathan and R. M. I. Betan, *J. Phys. G* **44** (2017) no.4, 045201 doi:10.1088/1361-6471/aa5f24 [arXiv:1601.06660 [nucl-th]].
- [93] J. J. He, S. Z. Chen, C. E. Rolfs, S. W. Xu, J. Hu, X. W. Ma, M. Wiescher, R. J. Deboer, T. Kajino and M. Kusakabe, *et al. Phys. Lett. B* **725** (2013), 287-291 doi:10.1016/j.physletb.2013.07.044
- [94] F. C. Barker, *Nucl. Phys. A* **707** (2002), 277-300 doi:10.1016/S0375-9474(02)00921-1
- [95] R. C. Johnson, *Phys. Lett. B* **114** (1982), 147-151 doi:10.1016/0370-2693(82)90134-4
- [96] W. Nortershauser, D. Tiedemann, M. Zakova, Z. Andjelkovic, K. Blaum, M. L. Bissell, R. Cazan, G. W. F. Drake, C. Geppert and M. Kowalska, *et al. Phys. Rev. Lett.* **102** (2009), 062503 doi:10.1103/PhysRevLett.102.062503 [arXiv:0809.2607 [nucl-ex]].
- [97] A. V. Dobrovolsky, G. A. Korolev, A. G. Inglessi, G. D. Alk hazov, G. Colò, I. Dillmann, P. Egelhof, A. Estradé, F. Farinon and H. Geissel, *et al. Nucl. Phys. A* **989** (2019), 40-58 doi:10.1016/j.nuclphysa.2019.05.012 [arXiv:1905.11399 [nucl-

- ex]].
- [98] I. Tanihata, H. Savajols and R. Kanungo, *Prog. Part. Nucl. Phys.* **68** (2013), 215-313 doi:10.1016/j.pnpnp.2012.07.001
- [99] S. L. Henderson, T. Ahn, M. A. Caprio, P. J. Fasano, A. Simon, W. Tan, P. O'Malley, J. Allen, D. W. Bardayan and D. Blankstein, *et al.* *Phys. Rev. C* **99** (2019) no.6, 064320 doi:10.1103/PhysRevC.99.064320 [[arXiv:2109.07312](#) [nucl-ex]].
- [100] N. J. Stone, *Atom. Data Nucl. Data Tabl.* **111-112** (2016), 1-28 doi:10.1016/j.adt.2015.12.002
- [101] C. W. Arnold, T. B. Clegg, C. Iliadis, H. J. Karwowski, G. C. Rich, J. R. Tompkins and C. R. Howell, *Phys. Rev. C* **85** (2012), 044605 doi:10.1103/PhysRevC.85.044605 [[arXiv:1112.1148](#) [nucl-ex]].
- [102] E. Kwan, C. Y. Wu, N. C. Summers, G. Hackman, T. E. Drake, C. Andreoiu, R. Ashley, G. C. Ball, P. C. Bender and A. J. Boston, *et al.* *Phys. Lett. B* **732** (2014), 210-213 doi:10.1016/j.physletb.2014.03.049
- [103] H. Iwasaki, T. Motobayashi, H. Akiyoshi, Y. Ando, N. Fukuda, H. Fujiwara, Z. Fülöp, K. I. Hahn, Y. Higurashi and M. Hirai, *et al.* *Phys. Lett. B* **491** (2000), 8-14 doi:10.1016/S0370-2693(00)01017-0
- [104] M. A. Caprio, P. J. Fasano and P. Maris, *Phys. Rev. C* **105** (2022) no.6, L061302 doi:10.1103/PhysRevC.105.L061302 [[arXiv:2206.09307](#) [nucl-th]].
- [105] J. N. Orce, T. E. Drake, M. K. Djongolov, P. Navratil, S. Triambak, G. C. Ball, H. Al Falou, R. Churchman, D. S. Cross and P. Finlay, *et al.* *Phys. Rev. C* **86** (2012), 041303 doi:10.1103/PhysRevC.86.041303
- [106] B. N. Lu, N. Li, S. Elhatisari, Y. Z. Ma, D. Lee and U.-G. Meißner, *Phys. Rev. Lett.* **128** (2022) no.24, 242501 doi:10.1103/PhysRevLett.128.242501 [[arXiv:2111.14191](#) [nucl-th]].
- [107] C. Hicks and D. Lee, *Phys. Rev. Res.* **5** (2023) no.2, L022001 doi:10.1103/PhysRevResearch.5.L022001 [[arXiv:2209.02083](#) [nucl-th]].
- [108] M. I. Abdulhamid *et al.* [STAR], *Nature* **635** (2024) no.8037, 67-72 doi:10.1038/s41586-024-08097-2 [[arXiv:2401.06625](#) [nucl-ex]].
- [109] Y. Kanada-En'yo, M. Kimura and A. Ono, *PTEP* **2012** (2012), 01A202 doi:10.1093/ptep/pts001 [[arXiv:1202.1864](#) [nucl-th]].

SUPPLEMENTAL MATERIAL

We give further information on the initial wave configurations, table of numerical values, and various numerical checks such as Euclidean time extrapolation, box size, and the breaking of cubic irrepresentation. All the results below are obtained by full N³LO interaction if not stated differently.

Euclidean time extrapolation

We use one exponential formulas for the extrapolation of observables. For the nonperturbative energy E_0 of the channel i , this reads:

$$E_0^{(i)}(\tau) = \frac{E_\infty^{(i)} + (E_\infty^{(i)} + d^{(i)})c^{(i)}e^{-d^{(i)}\tau}}{1 + c^{(i)}e^{-d^{(i)}\tau}}, \quad (\text{S1})$$

with E_∞ , c , and d the fit parameters.

For other observables, such as the energy and radius, we use

$$O^{(i)}(\tau) = \frac{O_\infty^{(i)} + O_1^{(i)}e^{-d^{(i)}\tau/2} + O_2^{(i)}e^{-d^{(i)}\tau}}{1 + c^{(i)}e^{-d^{(i)}\tau}}, \quad (\text{S2})$$

with O_∞ , O_1 , and O_2 as new fit parameters, while the parameters c and d will be fitted together with Eq. (S1). For observables with mixed channels such as transitions, the extrapolation formula is extended to

$$O^{(ij)}(\tau) = \frac{O_\infty^{(ij)} + O_1^{(i)}e^{-d^{(i)}\tau/2} + O_1^{(j)}e^{-d^{(j)}\tau/2}}{[1 + c^{(i)}e^{-d^{(i)}\tau}]^{1/2} [1 + c^{(j)}e^{-d^{(j)}\tau}]^{1/2}}. \quad (\text{S3})$$

Similarly to the above, the parameters c and d will be fitted together with Eq. (S1).

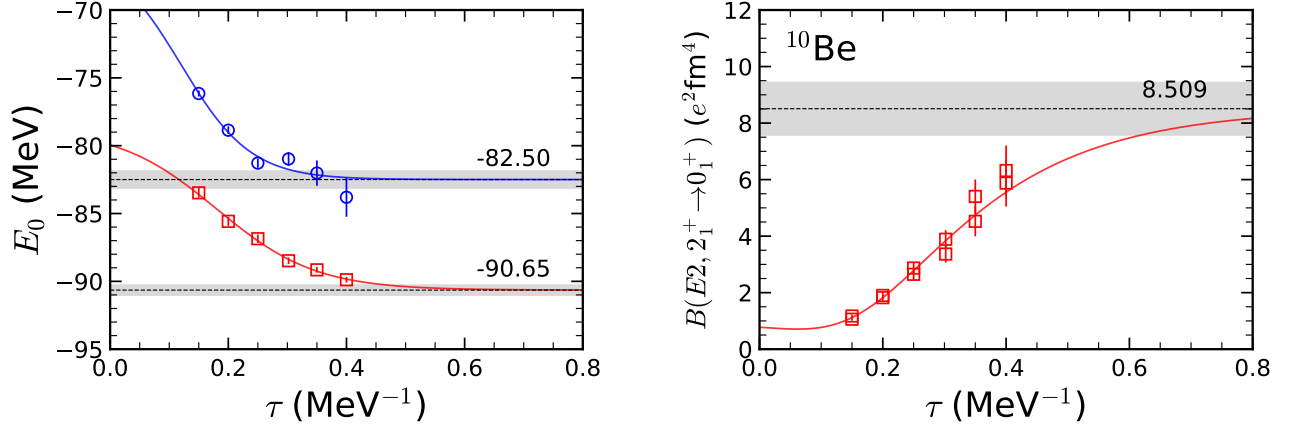


FIG. S1. (Left panel) Extrapolation of the nonperturbative energy of the 0_1^+ (red squares and lines) and 2_1^+ (blue circles and lines) states in ^{10}Be calculated in NLEFT. (Right panel) Extrapolation of $B(E2, 2_1^+ \rightarrow 0_1^+)$. The gray bands indicate the error of the parameters E_∞ and O_∞ .

As an example, in Fig. S1, we show the Euclidean time extrapolation of the nonperturbative energies and transition $B(E2, 2_1^+ \rightarrow 0_1^+)$ in ^{10}Be . The sign problem and computational complexity increase dramatically as the projection time τ increases, and therefore we will limit our resources to a reasonable range where the simulation gives reliable results. A multi-exponential extrapolation formula is not chosen to avoid overfitting.

Finite volume effect

We use two states that have a large spatial extension to show the finite volume effect: the first is the high-lying resonance $\frac{3}{2}^+$ in ${}^7\text{Be}$ and the second is the neutron halo state of $\frac{1}{2}^+$ in ${}^{11}\text{Be}$.

L [fm]	${}^7\text{Be}, E(\frac{3}{2}^+) [\text{MeV}]$	${}^{11}\text{Be}, E(\frac{1}{2}^+) [\text{MeV}]$
13.2	-31.6(6)	65.4(3)
15.7	-28.2(1.8)	65.3(6)

TABLE S1. Selected energies calculated at different box sizes L . The error bars indicate stochastic errors.

In Table S1 we show the results calculated at $L_t = 500$ for different box sizes. It can be seen for bound halo structure, the box size $L = 13.2$ fm is insufficient; while for unbound resonances, a mild finite volume effect can be seen. This can be improved in the future by better methods to address such type of states.

Rotational irrepresentation on lattice

Rotational symmetry including spin-1/2 particles on the lattice can be expressed by 8 irreducible representations (*irreps*): $A_1, A_2, E, T_1, T_2, G_1, G_2, H$ [1, 2]. Here we check how much the results are affected by the breaking of different *irreps*. We take the example of 2_1^+ in ${}^{10}\text{Be}$, with initial wave function of $J_z^\pi = 2^+$ shell-model wave function and can be both *irreps* of E^+ and T_2^+ . For energies the results are obtained at $L_t = 200$, and for $B(E2)$ at $L_t = 150$ due to large computational complexity. The comparison of two *irreps* E^+ and T_2^+ are listed in Table S2

<i>irrep</i>	$E(2_1^+) [\text{MeV}]$	$B(E2, 2_1^+ \rightarrow 0_1^+) [e^2\text{fm}^4]$
E^+	-61.6(3)	2.72(49)
T_2^+	-58.4(7)	1.95(61)

TABLE S2. Energy and $B(E2)$ transition of 2_1^+ in ${}^{10}\text{Be}$ for different *irreps*. The error bars indicate stochastic errors.

It can be seen the error due to breaking of different *irreps* is about 1.6 MeV in the energy and $0.38 e^2\text{fm}^4$ in the $B(E2)$ transitions. The results presented in the paper are obtained using $J_z = 2$ initial wave function without doing any *irrep* projection, therefore the two *irreps* are automatically averaged.

Initial wave function

A single Slater determinant composed of shell-model wave functions has been used as the initial wave function $|\Psi_0\rangle$ throughout this paper. Comparing with cluster wave function, the main advantage of using shell-model wave function is that a good quantum number J_z can be constructed and this helps to identify the total spin of the final state. With cluster wave function a projection into *irreps* is necessary and this often causes a severe sign problem.

In Table S3 we list the configurations we use for the initial wave function for different states. Note that the first 2 protons and neutrons always occupy the $1s_{1/2}$ orbital and therefore they are not listed. In some cases the order is not natural but is chosen for a numerical advantage (e.g. smaller error or lower energy), and since this is only a initial wave function, such change will not modify the final results. Furthermore, as there is no requirement of exact orthogonality, the single-particle wave function for each nucleon can be slightly adjusted to achieve a faster convergence such as using different harmonic oscillator strength.

TABLE S3: Proton ($p_i, i = 3, 4$) and neutron ($n_i, i = 3, \dots, N$) configuration of initial wave functions in NLEFT calculation for beryllium isotopes. The notation $l_j^{j_z}$ is used to denote the three quantum numbers l, j, j_z (orbital angular momentum, total angular momentum, projection of total angular momentum onto z -axis). The radial quantum number n is omitted to save space, for all p and d orbitals $n = 1$, while for all s orbitals $n = 2$. Projection of the total spin onto the z -axis and parity (J_z^π) are listed in the last column.

	p_3	p_4	n_3	n_4	n_5	n_6	n_7	n_8	J_z^π
${}^7\text{Be}, \frac{3}{2}^-$	$p_{3/2}^{+1/2}$	$p_{3/2}^{-1/2}$	$p_{3/2}^{+1/2}$						$\frac{3}{2}^-$
${}^7\text{Be}, \frac{1}{2}^-$	$p_{3/2}^{+1/2}$	$p_{3/2}^{-1/2}$	$p_{3/2}^{+3/2}$						$\frac{1}{2}^-$
${}^7\text{Be}, \frac{7}{2}^-$	$p_{1/2}^{+1/2}$	$p_{3/2}^{+3/2}$	$p_{3/2}^{+3/2}$						$\frac{7}{2}^-$
${}^7\text{Be}, (\frac{1}{2})^+$	$s_{1/2}^{+1/2}$	$p_{3/2}^{-1/2}$	$p_{3/2}^{+1/2}$						$\frac{1}{2}^+$
${}^7\text{Be}, (\frac{3}{2})^+$	$p_{3/2}^{+1/2}$	$s_{1/2}^{+1/2}$	$p_{3/2}^{+1/2}$						$\frac{3}{2}^+$
${}^7\text{Be}, (\frac{5}{2})^+$	$s_{1/2}^{+1/2}$	$p_{3/2}^{+3/2}$	$p_{3/2}^{+1/2}$						$\frac{5}{2}^+$
${}^8\text{Be}, 0_1^+$	$p_{3/2}^{+1/2}$	$p_{3/2}^{-1/2}$	$p_{3/2}^{+1/2}$	$p_{3/2}^{-1/2}$					0^+
${}^8\text{Be}, 2_1^+$	$p_{3/2}^{+1/2}$	$p_{3/2}^{+3/2}$	$p_{3/2}^{+1/2}$	$p_{3/2}^{-1/2}$					2^+
${}^8\text{Be}, 4_1^+$	$p_{3/2}^{+1/2}$	$p_{3/2}^{+3/2}$	$p_{3/2}^{+1/2}$	$p_{3/2}^{+3/2}$					4^+
${}^8\text{Be}, 2_1^-$	$p_{3/2}^{+1/2}$	$s_{1/2}^{-1/2}$	$p_{3/2}^{+1/2}$	$p_{3/2}^{-1/2}$					0^-
${}^9\text{Be}, \frac{3}{2}^-$	$p_{3/2}^{+1/2}$	$p_{3/2}^{-1/2}$	$p_{3/2}^{+1/2}$	$p_{3/2}^{-1/2}$	$p_{3/2}^{+3/2}$				$\frac{3}{2}^-$
${}^9\text{Be}, \frac{1}{2}^+$	$p_{3/2}^{+1/2}$	$p_{3/2}^{-1/2}$	$p_{3/2}^{+1/2}$	$p_{3/2}^{-1/2}$	$s_{1/2}^{+1/2}$				$\frac{1}{2}^+$
${}^9\text{Be}, \frac{5}{2}^-$	$p_{3/2}^{+3/2}$	$p_{3/2}^{-1/2}$	$p_{3/2}^{+1/2}$	$p_{3/2}^{-1/2}$	$p_{3/2}^{+3/2}$				$\frac{5}{2}^-$
${}^9\text{Be}, \frac{1}{2}^-$	$p_{3/2}^{+1/2}$	$p_{3/2}^{-1/2}$	$p_{3/2}^{+1/2}$	$p_{3/2}^{-3/2}$	$p_{3/2}^{+3/2}$				$\frac{1}{2}^-$
${}^9\text{Be}, \frac{5}{2}^+$	$p_{3/2}^{+1/2}$	$p_{3/2}^{-1/2}$	$p_{3/2}^{+1/2}$	$p_{3/2}^{-1/2}$	$d_{5/2}^{+5/2}$				$\frac{5}{2}^+$
${}^9\text{Be}, \frac{3}{2}^+$	$p_{3/2}^{+1/2}$	$p_{3/2}^{-1/2}$	$p_{3/2}^{+1/2}$	$p_{3/2}^{-1/2}$	$d_{5/2}^{+3/2}$				$\frac{3}{2}^+$
${}^9\text{Be}, \frac{7}{2}^-$	$p_{3/2}^{+1/2}$	$p_{3/2}^{+3/2}$	$p_{3/2}^{+1/2}$	$p_{3/2}^{-1/2}$	$p_{3/2}^{+3/2}$				$\frac{7}{2}^-$
${}^{10}\text{Be}, 0_1^+$	$p_{3/2}^{+1/2}$	$p_{3/2}^{-1/2}$	$p_{3/2}^{+1/2}$	$p_{3/2}^{-1/2}$	$p_{3/2}^{+3/2}$	$p_{3/2}^{-3/2}$			0^+
${}^{10}\text{Be}, 2_1^+$	$p_{3/2}^{+1/2}$	$p_{3/2}^{+3/2}$	$p_{3/2}^{+1/2}$	$p_{3/2}^{-1/2}$	$p_{3/2}^{+3/2}$	$p_{3/2}^{-3/2}$			2^+
${}^{10}\text{Be}, 2_2^+$	$p_{3/2}^{+1/2}$	$p_{3/2}^{-1/2}$	$p_{3/2}^{+1/2}$	$p_{3/2}^{-1/2}$	$p_{3/2}^{+3/2}$	$p_{1/2}^{+1/2}$			2^+
${}^{10}\text{Be}, 1_1^-$	$p_{3/2}^{+1/2}$	$p_{3/2}^{-1/2}$	$p_{3/2}^{+1/2}$	$p_{3/2}^{-1/2}$	$p_{1/2}^{+1/2}$	$s_{1/2}^{+1/2}$			1^-
${}^{10}\text{Be}, 0_2^+$	$p_{3/2}^{+1/2}$	$p_{3/2}^{-1/2}$	$p_{3/2}^{+1/2}$	$p_{3/2}^{-1/2}$	$s_{1/2}^{+1/2}$	$s_{1/2}^{-1/2}$			0^+
${}^{10}\text{Be}, 2_1^-$	$p_{3/2}^{+1/2}$	$p_{3/2}^{-1/2}$	$p_{3/2}^{+1/2}$	$p_{3/2}^{-1/2}$	$p_{3/2}^{+3/2}$	$s_{1/2}^{+1/2}$			2^-
${}^{10}\text{Be}, 3_1^-$	$p_{3/2}^{+1/2}$	$p_{3/2}^{-1/2}$	$p_{3/2}^{+1/2}$	$d_{5/2}^{+5/2}$	$p_{3/2}^{+3/2}$	$p_{3/2}^{+3/2}$			3^-
${}^{10}\text{Be}, A_1^+(3)$	$p_{3/2}^{+1/2}$	$p_{3/2}^{-1/2}$	$p_{3/2}^{+1/2}$	$p_{3/2}^{-1/2}$	$p_{1/2}^{+1/2}$	$p_{1/2}^{-1/2}$			0^+
${}^{10}\text{Be}, 2_3^+$	$p_{3/2}^{+1/2}$	$p_{3/2}^{-1/2}$	$p_{3/2}^{+1/2}$	$s_{1/2}^{-1/2}$	$p_{3/2}^{+3/2}$	$s_{1/2}^{+1/2}$			2^+
${}^{10}\text{Be}, (4_1^-)$	$p_{3/2}^{+1/2}$	$p_{3/2}^{-1/2}$	$p_{3/2}^{+1/2}$	$p_{3/2}^{-1/2}$	$p_{3/2}^{+3/2}$	$d_{5/2}^{+5/2}$			4^-
${}^{11}\text{Be}, \frac{1}{2}^+$	$p_{3/2}^{+1/2}$	$p_{3/2}^{-1/2}$	$p_{3/2}^{+1/2}$	$p_{3/2}^{-1/2}$	$p_{3/2}^{+3/2}$	$p_{3/2}^{-3/2}$	$s_{1/2}^{+1/2}$		$\frac{1}{2}^+$
${}^{11}\text{Be}, \frac{1}{2}^-$	$p_{3/2}^{+1/2}$	$p_{3/2}^{-1/2}$	$p_{3/2}^{+1/2}$	$p_{3/2}^{-1/2}$	$p_{3/2}^{+3/2}$	$p_{3/2}^{-3/2}$	$s_{1/2}^{+1/2}$		$\frac{1}{2}^-$
${}^{11}\text{Be}, \frac{5}{2}^+$	$p_{3/2}^{+1/2}$	$p_{3/2}^{-1/2}$	$p_{3/2}^{+1/2}$	$p_{3/2}^{-1/2}$	$p_{3/2}^{+3/2}$	$p_{3/2}^{-3/2}$	$d_{5/2}^{+5/2}$		$\frac{5}{2}^+$
${}^{11}\text{Be}, \frac{3}{2}^-$	$p_{3/2}^{+3/2}$	$p_{3/2}^{-1/2}$	$p_{3/2}^{+1/2}$	$p_{3/2}^{-1/2}$	$p_{3/2}^{+3/2}$	$p_{3/2}^{-3/2}$	$s_{1/2}^{+1/2}$		$\frac{3}{2}^-$
${}^{11}\text{Be}, (\frac{3}{2})^+$	$p_{3/2}^{+3/2}$	$p_{3/2}^{-1/2}$	$p_{3/2}^{+1/2}$	$p_{3/2}^{-1/2}$	$p_{3/2}^{+3/2}$	$p_{3/2}^{-3/2}$	$s_{1/2}^{+1/2}$		$\frac{3}{2}^+$
${}^{11}\text{Be}, \frac{5}{2}^-$	$p_{3/2}^{+1/2}$	$p_{3/2}^{+3/2}$	$p_{3/2}^{+1/2}$	$p_{3/2}^{-1/2}$	$p_{3/2}^{+3/2}$	$p_{3/2}^{-3/2}$	$s_{1/2}^{+1/2}$		$\frac{5}{2}^-$
${}^{12}\text{Be}, 0_1^+$	$p_{3/2}^{+1/2}$	$p_{3/2}^{-1/2}$	$p_{3/2}^{+1/2}$	$p_{3/2}^{-1/2}$	$p_{3/2}^{+3/2}$	$p_{3/2}^{-3/2}$	$p_{1/2}^{+1/2}$	$p_{1/2}^{-1/2}$	0^+
${}^{12}\text{Be}, 2_1^+$	$p_{3/2}^{+1/2}$	$p_{3/2}^{+3/2}$	$p_{3/2}^{+1/2}$	$p_{3/2}^{-1/2}$	$p_{3/2}^{+3/2}$	$p_{3/2}^{-3/2}$	$p_{1/2}^{+1/2}$	$p_{1/2}^{-1/2}$	2^+
${}^{12}\text{Be}, 0_2^+$	$p_{3/2}^{+1/2}$	$p_{3/2}^{-1/2}$	$p_{3/2}^{+1/2}$	$p_{3/2}^{-1/2}$	$p_{3/2}^{+3/2}$	$p_{3/2}^{-3/2}$	$s_{1/2}^{+1/2}$	$s_{1/2}^{-1/2}$	0^+
${}^{12}\text{Be}, 1_1^-$	$p_{3/2}^{+1/2}$	$p_{3/2}^{-1/2}$	$p_{3/2}^{+1/2}$	$p_{3/2}^{-1/2}$	$p_{3/2}^{+3/2}$	$p_{3/2}^{-3/2}$	$s_{1/2}^{+1/2}$	$s_{1/2}^{-1/2}$	1^-
${}^{12}\text{Be}, (2_1^-)$	$p_{3/2}^{+3/2}$	$p_{3/2}^{-1/2}$	$p_{3/2}^{+1/2}$	$p_{3/2}^{-1/2}$	$p_{3/2}^{+3/2}$	$p_{3/2}^{-3/2}$	$s_{1/2}^{+1/2}$	$s_{1/2}^{-1/2}$	2^-
${}^{12}\text{Be}, (2_2^+)$	$p_{3/2}^{+1/2}$	$p_{3/2}^{+3/2}$	$p_{3/2}^{+1/2}$	$p_{3/2}^{-1/2}$	$p_{3/2}^{+3/2}$	$p_{3/2}^{-3/2}$	$s_{1/2}^{+1/2}$	$s_{1/2}^{-1/2}$	2^+
${}^{12}\text{Be}, (3_1^-)$	$p_{3/2}^{+1/2}$	$p_{3/2}^{+3/2}$	$p_{3/2}^{+1/2}$	$p_{3/2}^{-1/2}$	$p_{3/2}^{+3/2}$	$p_{3/2}^{-3/2}$	$s_{1/2}^{+1/2}$	$s_{1/2}^{-1/2}$	3^-

Table of numerical values

Energies

In Table S4 we listed the numerical values of energies obtained by NLEFT using $N^3\text{LO}$ interaction [3] and SU(4) interaction [4].

TABLE S4: Energies of Be isotopes calculated by NLEFT using the SU(4) interaction [4] and $N^3\text{LO}$ interaction [3], compared to experiment [5–10]. All energies are in MeV. The error bars of NLEFT results are one standard deviation estimates due to stochastic errors and Euclidean time extrapolation.

	SU(4)	$N^3\text{LO}$	Exp.
${}^7\text{Be}, \frac{3}{2}^-$	-39.8(1)	-38.1(1)	-37.6
${}^7\text{Be}, \frac{1}{2}^-$	-39.5(1)	-37.9(1)	-37.2
${}^7\text{Be}, \frac{7}{2}^-$	-31.9(2)	-33.0(2)	-33.0
${}^7\text{Be}, (\frac{1}{2})^+$	-31.9(2)	-29.3(7)	-
${}^7\text{Be}, (\frac{3}{2})^+$	-29.9(3)	-31.1(8)	-
${}^7\text{Be}, (\frac{5}{2})^+$	-26.5(1)	-26.8(3)	-
${}^8\text{Be}, 0^+$	-56.6(1)	-56.7(4)	-56.5
${}^8\text{Be}, 2^+$	-52.7(1)	-54.0(3)	-53.5
${}^8\text{Be}, 4^+$	-46.2(1.9)	-45.9(1.2)	-45.1
${}^8\text{Be}, 2^-$	-39.3(3)	-40.4(4)	-37.6
${}^9\text{Be}, \frac{3}{2}^-$	-56.2(1)	-57.6(3)	-58.2
${}^9\text{Be}, \frac{1}{2}^+$	-56.5(2)	-56.8(5)	-56.5
${}^9\text{Be}, \frac{5}{2}^-$	-53.9(1)	-55.3(6)	-55.7
${}^9\text{Be}, \frac{7}{2}^-$	-55.9(1)	-56.7(5)	-55.4
${}^9\text{Be}, \frac{3}{2}^+$	-53.2(2)	-55.3(4)	-55.1
${}^9\text{Be}, \frac{5}{2}^+$	-55.1(6)	-53.9(2)	-53.5
${}^9\text{Be}, \frac{7}{2}^-$	-49.7(3)	-51.7(6)	-51.8
${}^{10}\text{Be}, 0^+$	-64.1(1)	-63.7(3)	-65.0
${}^{10}\text{Be}, 2^+$	-60.2(1)	-61.0(3)	-61.6
${}^{10}\text{Be}, 2^+$	-59.1(1)	-60.3(3)	-59.0
${}^{10}\text{Be}, 1^-$	-57.3(2)	-58.9(9)	-59.0
${}^{10}\text{Be}, 0^+$	-58.0(2)	-59.5(1.1)	-58.8
${}^{10}\text{Be}, 2^-$	-56.8(3)	-58.5(6)	-58.7
${}^{10}\text{Be}, 3^-$	-56.2(3)	-57.8(4)	-57.6
${}^{10}\text{Be}, 2^+$	-57.0(1)	-59.8(3)	-57.4
${}^{10}\text{Be}, A_1^+(3)$	-56.1(7)	-58.4(9)	-
${}^{10}\text{Be}, (4^-)$	-52.4(1)	-55.1(9)	-55.7
${}^{11}\text{Be}, \frac{1}{2}^+$	-64.6(1)	-65.6(5)	-65.5
${}^{11}\text{Be}, \frac{1}{2}^-$	-64.1(1)	-63.5(13)	-65.2
${}^{11}\text{Be}, \frac{5}{2}^+$	-60.7(1)	-61.2(3)	-63.7
${}^{11}\text{Be}, \frac{3}{2}^-$	-63.4(1)	-62.6(1)	-62.8
${}^{11}\text{Be}, (\frac{3}{2})^+$	-60.1(2)	-61.4(3)	-62.1 ¹
${}^{11}\text{Be}, \frac{5}{2}^-$	-59.4(3)	-63.4(13)	-61.6
${}^{12}\text{Be}, 0^+$	-72.0(1)	-68.0(4)	-68.6
${}^{12}\text{Be}, 2^+$	-67.7(2)	-66.1(6)	-66.5
${}^{12}\text{Be}, 0^+$	-66.8(1)	-64.8(11)	-66.4
${}^{12}\text{Be}, 1^-$	-65.4(1)	-66.9(1)	-65.9
${}^{12}\text{Be}, (2^-)$	-62.1(5)	-60.3(3)	-64.2
${}^{12}\text{Be}, (2^+)$	-64.6(7)	-64.2(4)	-63.8
${}^{12}\text{Be}, (3^-)$	-60.9(1)	-62.4(9)	-62.9 ²

¹ For Exp., $(\frac{3}{2}^+, \frac{3}{2}^-)$

² For Exp., $(4^+, 2^+, 3^-)$

Radii

In Table S5, we give the values of the calculated charge and matter radii in comparison to experiment.

TABLE S5. Energies of Be isotopes calculated by NLEFT using the SU(4) interaction [4] and N³LO interaction [3], compared to experiment. All energies are in MeV and radii in fm. For the NLEFT results, the error bars are one standard deviation estimates due to stochastic errors and Euclidean time extrapolation.

r_c (fm)	SU(4)	N ³ LO	Exp. [11, 12]
⁷ Be	2.557(3)	2.580(18)	2.647(17)
⁹ Be	2.576(8)	2.552(16)	2.519(12)
¹⁰ Be	2.466(5)	2.511(37)	2.357(18)
¹¹ Be	2.576(4)	2.543(41)	2.463(16)
¹² Be	2.352(2)	2.579(34)	2.503(15)
r_m (fm)	NLEFT, SU(4)	NLEFT, N ³ LO	Exp. [13, 14]
⁷ Be	2.37(1)	2.39(1)	2.42(4)
⁹ Be	2.60(1)	2.52(1)	2.38(1)
¹⁰ Be	2.48(1)	2.53(2)	2.30(2)
¹¹ Be	3.14(1)	2.86(1)	2.91(5)
¹² Be	2.45(1)	2.63(1)	2.59(6)

Comparison of transition properties

In Table S6, we give the values of the calculated transition properties in comparison to experiment.

⁷ Be	Exp. [15]	N ³ LO	SU(4)	NCSMC [16]	NCFC [17]	GFMC [18, 19]			
$E2, \frac{3}{2}^- \rightarrow \frac{1}{2}^-$	26(6)(3)	15.2(5)	16.0(2)	20.0	19.3	22.2(11)–27.5(8)			
⁹ Be	Exp. [9]	NLEFT	SU(4)	CSM [20]	AMD [21]	GFMC [19, 22]	NCSM [23]	MMM [24]	
$Q(\frac{3}{2}^-)$	5.29(4) [25]	7.4(1.0)	7.3(1)	5.30		5.0(3)–8.5(3)			
$E1, \frac{1}{2}^+ \rightarrow \frac{3}{2}^-$	0.136(2) [26]	0.060(15)	0.131(3)	0.048	0.002		0.033	0.061	
$E1, \frac{3}{2}^+ \rightarrow \frac{1}{2}^-$	0.010(8)	0.049(5)	0.045(14)	0.005	0.013		0.006	0.025	
$E2, \frac{5}{2}^- \rightarrow \frac{3}{2}^-$	27.1(2.0)	27.8(1.9)	35.7(1.8)	23.9		25.6(6)		17.6(6)	
$E2, \frac{7}{2}^- \rightarrow \frac{5}{2}^-$	9.5(4.1)	5.3(8)	11.6(2.5)	10.0					
¹⁰ Be	Exp. [9]	NLEFT	SU(4)	Multicool [27]	GCM [28]	NCSM [29]	MCSM [30]	GFMC [31]	MO [32]
$E1, 3_1^- \rightarrow 2_1^+$	0.009(1)	0.004(3)	0.026(2)						
$E2, 2_1^+ \rightarrow 0_1^+$	9.2(3) [31]	8.5(9)	10.6(4)	7.9	5.66	9.8	9.3	8.1(3)–17.9(5)	11.26
¹¹ Be	Exp. [33]	NLEFT	SU(4)	NCSMC [34]	AMD [35]	GCM [28]			
$E1, \frac{1}{2}^- \rightarrow \frac{1}{2}^+$	0.102(2)	0.038(3)	0.023(3)	0.117–0.146	0.61–0.73	0.002			
¹² Be	Exp.	NLEFT	SU(4)	FMD [11]	GCM [36]	NCSM [36]	HAEM [37]	AMD [38]	
$E1, 0_1^+ \rightarrow 1_1^-$	0.051(13)[39]	0.056(26)	0.049(2)				0.046–0.064		
$E2, 2_1^+ \rightarrow 0_1^+$	14.2(1.0)(2.0)[40]	9.0(3.1)	7.8(1.1)	8.75	12.6	3.5–4.6	3.04–3.93	14	

TABLE S6. Quadrupole moments and transition rates of Be isotopes calculated using NLEFT with the N³LO interaction [3] and the SU(4) interaction [4], compared to experimental data and other theoretical models. Units: Q and $m(E0)$ in efm^2 , $B(E1)$ in e^2fm^2 , and $B(E2)$ in e^2fm^4 . For results presented as ranges, the ranges reflect variations from different interactions and numerical methods.

Intrinsic density

There is no fixed definition of the one-body intrinsic density, $\rho(\mathbf{r})$, derived from the many-body density, $\rho(\mathbf{r}_1, \mathbf{r}_2, \dots, \mathbf{r}_A)$. A common approach is to align each configuration along the principal axis [41]. However, this alignment can artificially enhance the prominence of the principal axis. In our study of neutron-rich Beryllium isotopes, we observe that this method tends to position the valence neutrons along the long principal axis, as they are often located far from the center.

Building on our previous work with ¹²C [4], we introduce an α -cluster-view intrinsic density, illustrated in schematic Figure S2. Similar to Ref. [4], we first group the nucleons into N_α clusters by considering all possible permutations of protons

and neutrons and selecting the arrangement that minimizes the sum of inter-nucleon distances. We then determine the symmetry axis for each configuration; however, this axis is not uniquely defined and depends on the specific system under investigation. For example, in ${}^8\text{Be}$, identifying the symmetry axis as the z -axis is straightforward because the two clusters always align linearly. In contrast, for ${}^9\text{Be}$, the presence of a valence neutron introduces an angle between the clusters, resulting in an angle $(\alpha_1, 0, \alpha_2) < 180^\circ$. This approach can be generalized to other nuclei, such as the ground state of ${}^{12}\text{C}$, where the symmetry axis is defined based on an equilateral triangular arrangement of three clusters [4]. However, in each configuration, two clusters are typically closer together than the third, allowing the symmetry axis to also be defined based on an acute triangular arrangement rather than an equilateral one. Therefore, the choice of symmetry axis depends on the specific problem and the perspective adopted. In this study, we consistently define the symmetry axis of Beryllium isotopes as the z -axis and randomly select one cluster to align along the positive or negative z direction.

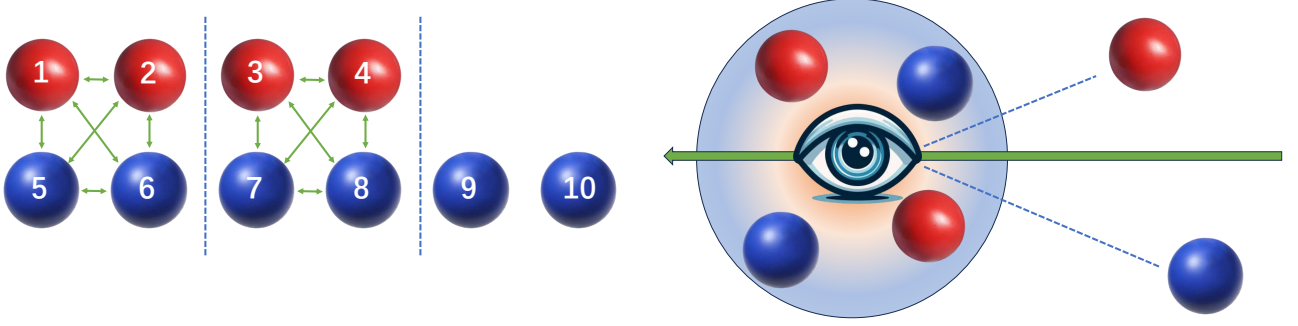


FIG. S2. Schematic show of grouping clusters and the intrinsic density from the view of cluster.

In Figure S3, we present the total density derived using the previously introduced α -cluster-view intrinsic density. The general features observed from ${}^8\text{Be}$ to ${}^{12}\text{Be}$ have been discussed in the main text and show good agreement with results from other studies. Specifically, for ${}^7\text{Be}$, the characteristic ${}^4\text{He}$ plus ${}^3\text{He}$ clustering is effectively captured by the α -cluster-view intrinsic density. In the case of the ambiguous positive-parity state of ${}^7\text{Be}$, one proton is excited out of the ${}^3\text{He}$ cluster. This excitation disrupts the small cluster, leading to significant shape deformation and spatial extension, as illustrated by the β_{pin} and γ_{pin} plots in the main text. Similarly, for the 2_1^- state of ${}^8\text{Be}$, one proton is excited out of the α cluster. This results in a very high excitation energy and a substantial change in the nuclear shape. In the present study, the third component of the total spin is fixed at $J_z = J$. Exploring the J_z -dependence of the structure would be an interesting avenue for future investigation.

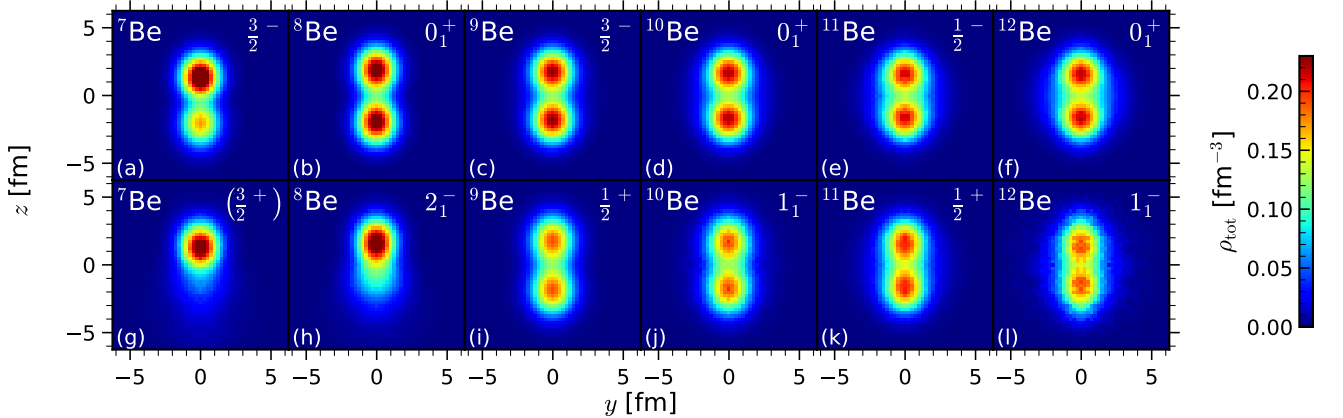


FIG. S3. Intrinsic density at $x = 0$ plane of selected states of beryllium isotopes obtained by NLEFT using N^3LO interaction. The third component of total spin is fixed at $J_z = J$.

In Figure S4, we display the density distributions of valence particles obtained using the previously introduced α -cluster-view intrinsic density. For ${}^7\text{Be}$, these valence particles consist of two protons and one neutron that are not grouped into the α cluster. In contrast, for the other isotopes, the valence particles are neutrons. To maintain a consistent color scale across all panels, we

normalized the density distributions differently for each case. For example, in the ${}^7\text{Be}$ $3/2^-$ state, the ${}^3\text{He}$ cluster exhibits a much higher concentration, necessitating division by a larger normalization factor. The features of the π and σ orbitals, which are discussed in detail in the main text, are more clearly observable in the ${}^9\text{Be}$ case, as shown in panels (b) and (d). The low probability regions at small z and large y coordinates may be attributed to the finite Euclidean time projection used in our calculations. Due to the sign problem, the computations cannot extend to larger L_t values and are limited to $L_t = 300$. Remarkably, starting from a common shell-model initial wavefunction, distinct nuclear molecular orbitals emerge automatically. The severity of the sign problem generally increases with the number of nucleons and for states with unnatural parity, resulting in larger errors in the valence particle densities compared to the total densities. Consequently, the uneven density distributions plotted, such as those in panel (j) of Fig. S4, are purely due to statistical errors.

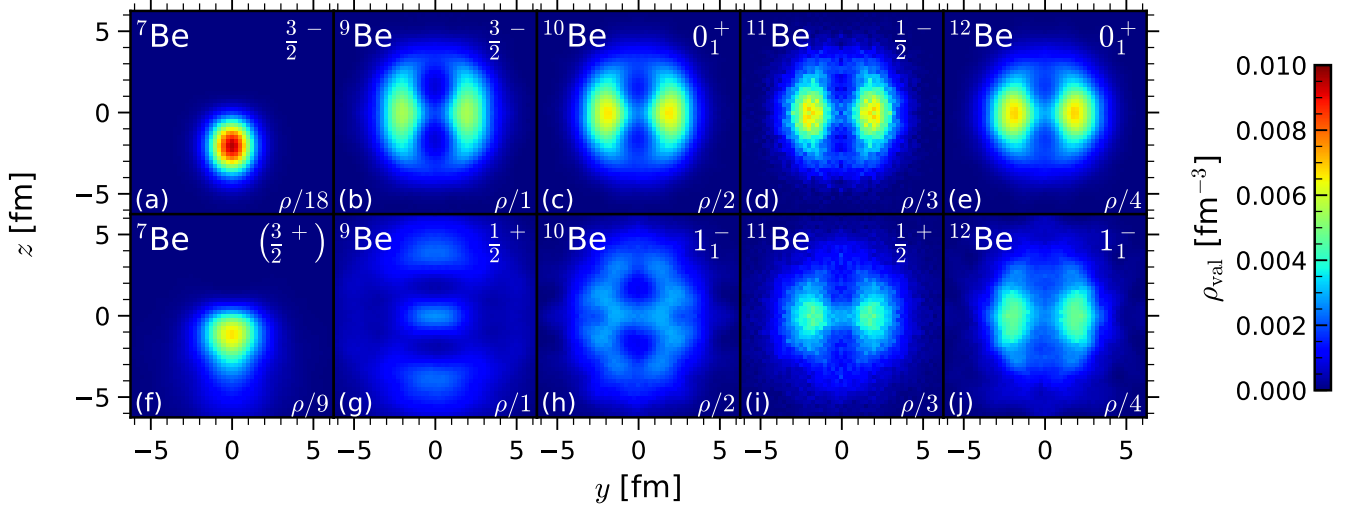


FIG. S4. Intrinsic density at $x = 0$ plane of selected states of beryllium isotopes obtained by NLEFT using N^3LO interaction. The third component of total spin is fixed at $J_z = J$.

* meissner@hiskp.uni-bonn.de

- [1] R. C. Johnson, Phys. Lett. B **114** (1982), 147-151 doi:10.1016/0370-2693(82)90134-4
- [2] B. N. Lu, T. A. Lähde, D. Lee and U.-G. Meißner, Phys. Rev. D **90** (2014) no.3, 034507 doi:10.1103/PhysRevD.90.034507 [arXiv:1403.8056 [nucl-th]].
- [3] S. Elhatisari, L. Bovermann, Y. Z. Ma, E. Epelbaum, D. Frame, F. Hildenbrand, M. Kim, Y. Kim, H. Krebs and T. A. Lähde, *et al.* Nature **630** (2024) no.8015, 59-63 doi:10.1038/s41586-024-07422-z [arXiv:2210.17488 [nucl-th]].
- [4] S. Shen, S. Elhatisari, T. A. Lähde, D. Lee, B. N. Lu and U.-G. Meißner, Nature Commun. **14** (2023) no.1, 2777 [arXiv:2202.13596 [nucl-th]].
- [5] W. Liu, J. L. Lou, Y. L. Ye, S. M. Wang, Z. W. Tan, Z. H. Li, Q. T. Li, H. Hua, X. F. Yang and J. Y. Xu, *et al.* Phys. Rev. C **105** (2022) no.3, 034613 doi:10.1103/PhysRevC.105.034613
- [6] M. Wang, W. J. Huang, F. G. Kondev, G. Audi and S. Naimi, Chin. Phys. C **45** (2021) no.3, 030003 doi:10.1088/1674-1137/abddaf
- [7] J. H. Kelley, J. E. Purcell and C. G. Sheu, Nucl. Phys. A **968** (2017), 71-253 doi:10.1016/j.nuclphysa.2017.07.015
- [8] J. H. Kelley, E. Kwan, J. E. Purcell, C. G. Sheu and H. R. Weller, Nucl. Phys. A **880** (2012), 88-195 doi:10.1016/j.nuclphysa.2012.01.010
- [9] D. R. Tilley, J. H. Kelley, J. L. Godwin, D. J. Millener, J. E. Purcell, C. G. Sheu and H. R. Weller, Nucl. Phys. A **745** (2004), 155-362 doi:10.1016/j.nuclphysa.2004.09.059
- [10] D. R. Tilley, C. M. Cheves, J. L. Godwin, G. M. Hale, H. M. Hofmann, J. H. Kelley, C. G. Sheu and H. R. Weller, Nucl. Phys. A **708** (2002), 3-163 doi:10.1016/S0375-9474(02)00597-3
- [11] A. Krieger, K. Blaum, M. L. Bissell, N. Frommgen, C. Geppert, M. Hammen, K. Kreim, M. Kowalska, J. Kramer and T. Neff, *et al.* Phys. Rev. Lett. **108** (2012), 142501 doi:10.1103/PhysRevLett.108.142501 [arXiv:1202.4873 [physics.atom-ph]].
- [12] W. Nortershauser, D. Tiedemann, M. Zakova, Z. Andjelkovic, K. Blaum, M. L. Bissell, R. Cazan, G. W. F. Drake, C. Geppert and M. Kowalska, *et al.* Phys. Rev. Lett. **102** (2009), 062503 doi:10.1103/PhysRevLett.102.062503 [arXiv:0809.2607 [nucl-ex]].
- [13] A. V. Dobrovolsky, G. A. Korolev, A. G. Inglessi, G. D. Alkhazov, G. Colò, I. Dillmann, P. Egelhof, A. Estradé, F. Farinon and H. Geissel, *et al.* Nucl. Phys. A **989** (2019), 40-58 doi:10.1016/j.nuclphysa.2019.05.012 [arXiv:1905.11399 [nucl-ex]].
- [14] I. Tanihata, H. Savajols and R. Kanungo, Prog. Part. Nucl. Phys. **68** (2013), 215-313 doi:10.1016/j.pnpnp.2012.07.001

- [15] S. L. Henderson, T. Ahn, M. A. Caprio, P. J. Fasano, A. Simon, W. Tan, P. O'Malley, J. Allen, D. W. Bardayan and D. Blankstein, *et al.* Phys. Rev. C **99** (2019) no.6, 064320 doi:10.1103/PhysRevC.99.064320 [arXiv:2109.07312 [nucl-ex]].
- [16] M. Vorabbi, P. Navrátil, S. Quaglioni and G. Hupin, Phys. Rev. C **100** (2019) no.2, 024304 doi:10.1103/PhysRevC.100.024304 [arXiv:1906.09258 [nucl-th]].
- [17] T. Heng, J. P. Vary and P. Maris, Phys. Rev. C **95** (2017) no.1, 014306 doi:10.1103/PhysRevC.95.014306 [arXiv:1602.00156 [nucl-th]].
- [18] M. Pervin, S. C. Pieper and R. B. Wiringa, Phys. Rev. C **76** (2007), 064319 doi:10.1103/PhysRevC.76.064319 [arXiv:0710.1265 [nucl-th]].
- [19] S. Pastore, S. C. Pieper, R. Schiavilla and R. B. Wiringa, Phys. Rev. C **87** (2013) no.3, 035503 doi:10.1103/PhysRevC.87.035503 [arXiv:1212.3375 [nucl-th]].
- [20] V. Della Rocca and F. Iachello, Nucl. Phys. A **973** (2018), 1-32 doi:10.1016/j.nuclphysa.2018.02.003
- [21] Y. Kanada-En'yo, Phys. Rev. C **93** (2016) no.2, 024322 doi:10.1103/PhysRevC.93.024322 [arXiv:1511.08530 [nucl-th]].
- [22] S. C. Pieper, K. Varga and R. B. Wiringa, Phys. Rev. C **66** (2002), 044310 doi:10.1103/PhysRevC.66.044310 [arXiv:nucl-th/0206061 [nucl-th]].
- [23] C. Forssen, P. Navratil, W. E. Ormand and E. Caurier, Phys. Rev. C **71** (2005), 044312 doi:10.1103/PhysRevC.71.044312 [arXiv:nucl-th/0412049 [nucl-th]].
- [24] K. Arai, P. Descouvemont, D. Baye and W. N. Catford, Phys. Rev. C **68** (2003), 014310 doi:10.1103/PhysRevC.68.014310
- [25] N. J. Stone, Atom. Data Nucl. Data Tabl. **111-112** (2016), 1-28 doi:10.1016/j.adt.2015.12.002
- [26] C. W. Arnold, T. B. Clegg, C. Iliadis, H. J. Karwowski, G. C. Rich, J. R. Tompkins and C. R. Howell, Phys. Rev. C **85** (2012), 044605 doi:10.1103/PhysRevC.85.044605 [arXiv:1112.1148 [nucl-ex]].
- [27] T. Myo, M. Lyu, Q. Zhao, M. Isaka, N. Wan, H. Takemoto and H. Horiuchi, Phys. Rev. C **108** (2023) no.6, 064314 doi:10.1103/PhysRevC.108.064314 [arXiv:2311.16391 [nucl-th]].
- [28] P. Descouvemont and N. Itagaki, PTEP **2020** (2020) no.2, 023D02 doi:10.1093/ptep/ptz169
- [29] J. N. Orce, T. E. Drake, M. K. Djongolov, P. Navratil, S. Triambak, G. C. Ball, H. Al Falou, R. Churchman, D. S. Cross and P. Finlay, *et al.* Phys. Rev. C **86** (2012), 041303 doi:10.1103/PhysRevC.86.041303
- [30] L. Liu, T. Otsuka, N. Shimizu, Y. Utsuno and R. Roth, Phys. Rev. C **86** (2012), 014302 doi:10.1103/PhysRevC.86.014302 [arXiv:1105.2983 [nucl-th]].
- [31] E. A. McCutchan, C. J. Lister, R. B. Wiringa, S. C. Pieper, D. Seweryniak, J. P. Greene, M. P. Carpenter, C. J. Chiara, R. V. F. Janssens and T. L. Khoo, *et al.* Phys. Rev. Lett. **103** (2009), 192501 doi:10.1103/PhysRevLett.103.192501 [arXiv:0907.3688 [nucl-ex]].
- [32] N. Itagaki and S. Okabe, Phys. Rev. C **61** (2000), 044306 doi:10.1103/PhysRevC.61.044306
- [33] E. Kwan, C. Y. Wu, N. C. Summers, G. Hackman, T. E. Drake, C. Andreoiu, R. Ashley, G. C. Ball, P. C. Bender and A. J. Boston, *et al.* Phys. Lett. B **732** (2014), 210-213 doi:10.1016/j.physletb.2014.03.049
- [34] A. Calci, P. Navrátil, R. Roth, J. Dohet-Eraly, S. Quaglioni and G. Hupin, Phys. Rev. Lett. **117** (2016) no.24, 242501 doi:10.1103/PhysRevLett.117.242501 [arXiv:1608.03318 [nucl-th]].
- [35] M. Dan, R. Chatterjee and M. Kimura, Eur. Phys. J. A **57** (2021) no.6, 203 doi:10.1140/epja/s10050-021-00526-4 [arXiv:2101.02885 [nucl-th]].
- [36] M. Dufour, P. Descouvemont and F. Nowacki, Nucl. Phys. A **836** (2010), 242-255 doi:10.1016/j.nuclphysa.2010.02.002
- [37] C. Romero-Redondo, E. Garrido, D. V. Fedorov and A. S. Jensen, Phys. Rev. C **77** (2008), 054313 doi:10.1103/PhysRevC.77.054313 [arXiv:0804.2351 [nucl-th]].
- [38] Y. Kanada-En'yo and H. Horiuchi, Phys. Rev. C **68** (2003), 014319 doi:10.1103/PhysRevC.68.014319 [arXiv:nucl-th/0301059 [nucl-th]].
- [39] H. Iwasaki, T. Motobayashi, H. Akiyoshi, Y. Ando, N. Fukuda, H. Fujiwara, Z. Fülöp, K. I. Hahn, Y. Higurashi and M. Hirai, *et al.* Phys. Lett. B **491** (2000), 8-14 doi:10.1016/S0370-2693(00)01017-0
- [40] C. Morse, E. A. McCutchan, H. Iwasaki, C. J. Lister, V. M. Bader, D. Bazin, S. Beceiro Novo, P. Chowdhury, A. Gade and T. D. Johnson, *et al.* Phys. Lett. B **780** (2018), 227-232 doi:10.1016/j.physletb.2018.03.004
- [41] R. B. Wiringa, S. C. Pieper, J. Carlson and V. R. Pandharipande, Phys. Rev. C **62** (2000), 014001 doi:10.1103/PhysRevC.62.014001 [arXiv:nucl-th/0002022 [nucl-th]].

* meissner@hiskp.uni-bonn.de